

Quantum Criticality Enabled by Intertwined Degrees of Freedom

Chia-Chuan Liu^{1,2}, Silke Paschen^{3,1}, and Qimiao Si^{1,*}

¹ Department of Physics and Astronomy, Rice Center for Quantum Materials, Rice University, Houston, Texas 77005, USA

² Département de Physique, Université de Montréal, Québec, H3C 3J7, Canada

³Institute of Solid State Physics, Vienna University of Technology, 1040 Vienna, Austria

Strange metals appear in a wide range of correlated materials. Electronic localization-delocalization and the expected loss of quasiparticles characterize beyond-Landau metallic quantum critical points and the associated strange metals. Typical settings involve local spins. Systems that contain entwined degrees of freedom offer new platforms to realize novel forms of quantum criticality. Here, we study the fate of an SU(4) spin-orbital Kondo state in a multipolar Bose-Fermi Kondo model, which provides an effective description of a multipolar Kondo lattice, using a renormalization-group method. We show that at zero temperature a generic trajectory in the model's parameter space contains two quantum critical points, which are associated with the destruction of Kondo entanglement in the orbital and spin channels respectively. Our asymptotically exact results reveal an overall phase diagram, provide the theoretical basis to understand puzzling recent experiments of a multipolar heavy fermion metal, and point to a means of designing new forms of quantum criticality and strange metallicity in a variety of strongly correlated systems.

Significance Statement: *Melting ice illustrates how phase transitions occur by varying temperature. Quantum phase transitions appear at absolute zero temperature, when the extent to which Heisenberg's uncertainty principle affects matter is tuned through a control parameter. For a continue transition, quantum criticality arises and influences the physics over a wide parameter range at finite temperatures. In quantum materials, the microscopic agent for quantum criticality is usually spin. Here we show that intertwining spins, orbitals and other degrees of freedom provides a means to design novel forms of quantum criticality. Our work provides the understanding of puzzling recent experiments in a spin-orbital-entwined heavy fermion metal, and promises to realize new types of quantum criticality in a variety of strongly correlated metals.*

Simple metals such as copper and aluminum are well described in terms of weakly correlated itinerant electrons. In a wide range of strongly correlated metals, the electrons' Coulomb repulsion is comparable to or larger than their bandwidth [1, 2]. The strong correlations are expected to cause a loss of Landau quasiparticles and the associated strange metallicity [3, 4]. Correlations turn certain bare electrons into effective local degrees of freedom in the building blocks for the low-energy physics. A prototypical case is the heavy fermion metals, which feature a wide variety of quantum phases [5–7]. Here, local spins are associated with the correlated $4f$ -electrons. Their entanglement with the background conduction electrons gives rise to the spin-isotropic [SU(2)-symmetric] Kondo effect [8]. The destruction of the Kondo effect corresponds to a localization of the $4f$ -electrons, is expected to cause a loss of quasiparticles, and represents a prototype mechanism for strange metallicity and beyond-Landau quantum critical points (QCPs) [9–17].

The notion that local correlation effects drive new forms of quantum fluctuations raises the possibility of designing new types of quantum criticality by controlling local degrees of freedom. For the Kondo effect *per se*, various kinds of local degrees of freedom have led to a variety of Kondo states relevant to multipolar heavy fermion metals [18–25], multi-orbital iron-based compounds [26–29], synthetic systems such as ultracold atoms [30] and mesoscopic devices [31–33], and other correlated settings [34–37]. Recent experiments [38, 39] have motivated the idea [40, 41] that, through molecular orbitals (of limited spatial extent), Kondo effects develop as a proper description of the low-energy physics even for d -electron-based flat band systems. Meanwhile, in twisted graphene structures, there have been proposals for their understanding in terms of Kondo effects that are associated with the degrees of freedom of moiré unit cells [42–44]. In these systems, different kinds of crystalline symmetries or stacking/twisting in different types of flat bands can yield various forms of local degrees of freedom. In heavy fermion metals, the nature of the local degrees of freedom is controlled by the cooperation of strong correlations, large spin-orbit coupling and crystalline symmetry. Indeed, there is a growing list of heavy fermion metals in which the role of multipolar degrees of freedom has been explored for their quantum criticality [2, 45]. These include $\text{Pr(TM)}_2\text{Al}_{20}$ (TM = Ti, V), which have non-magnetic doublets in the ground-state manifold [46, 47], $\text{PrOs}_4\text{Sb}_{12}$, which involves field-induced local quadrupolar moments [48, 49], and YbRu_2Ge_2 , which hosts quasi-degenerate spin and higher-rank moments [50, 51].

The hope of advancing this design principle for new types of quantum criticality is in particular triggered by recent experimental studies [52] on a heavy fermion compound $\text{Ce}_3\text{Pd}_{20}\text{Si}_6$ (Ref.53) as a function of a non-thermal control parameter (magnetic field). Surprisingly, the experimental

results show *two stages* of Kondo-destruction quantum criticality [see the Supplementary Information (SI), Sec. A]. In this system, the $4f$ electrons form a total angular momentum $J = 5/2$ state whose six-fold degeneracy is further split as dictated by the point-group symmetry [54]. What lies in the ground-state manifold is the Γ_8 quartet [55], which can be represented in the pseudo-spin $\vec{\sigma}$ and pseudo-orbital $\vec{\tau}$ bases (see the SI, Sec. A). The competition between the Kondo entanglement in the Γ_8 -manifold and the associated RKKY interactions may therefore be responsible for this sequential Kondo destruction.

The striking experimental observations motivate a well-defined theoretical question: what is the generic type of QCPs that result from this type of competition? The minimal prototype model of interest is the spin-orbital entwined multipolar Bose-Fermi Kondo model (BFK) [52, 56], as illustrated in Fig. 1. It is an effective model that emerges in the extended dynamical mean field theory of the multipolar Kondo lattice (see the SI, Sec. B). The model involves the local degrees of freedom, containing both the spin σ and the orbital τ components, which are coupled to the fermionic and bosonic baths. The former couplings describe the (fermionic) Kondo effect, while the latter describes the collective fluctuations associated with the RKKY interactions. An outstanding question is whether a generic tuning trajectory leads to two-stage transitions or whether it could also involve a one-stage transition. We focus on a multipolar Bose-Fermi Kondo model that arises as an effective Hamiltonian of the multipolar Kondo lattice model through the extended dynamical mean field theory [56–59] (SI, Sec. B). In addition, we take advantage of the understanding on spin-only systems, namely the emergence of new fixed points in the Bose-Fermi Kondo model is insensitive to the spin symmetry [56, 60] and, furthermore, the Kondo destruction fixed points of the Bose-Fermi model are realized in the corresponding Kondo lattice model through the extended dynamical mean field analysis. Accordingly, we i) will analyze the multipolar Bose-Fermi Kondo model in its Ising-anisotropic case to allow for comprehensive analytical studies, though we expect that the conclusion that new fixed points develop in this model will apply to the spin-isotropic case as well and ii) expect that the new fixed points that we identify in the multipolar Bose-Fermi Kondo model will be realized as Kondo destruction quantum critical points in the multipolar Kondo lattice model.

We thus study the multipolar Bose-Fermi Kondo model at zero temperature. By using a Coulomb-gas representation of the Bose-Fermi Kondo model, we carry out analytical renormalization-group (RG) calculations that are controlled by an expansion in terms of a small quantity ϵ (defined in Eq. 3). We uncover an overall phase diagram at zero temperature, which reveals the mecha-

nism for the sequential Kondo destruction and shows that it appears for any generic trajectory in the phase diagram. Our asymptotically exact theory points to a new design principle for beyond-Landau quantum criticality and strange metallicity in a variety of other strongly correlated systems, including d -electron-based flat band systems and moiré structures.

Results

Sequential Destruction of Multipolar Kondo Entanglement. Our key findings are visualized in terms of an overall phase diagram presented in the $g_{\sigma z}$ - $g_{\tau z}$ parameter space, as illustrated in Fig. 2. Here, $g_{\sigma z}$ and $g_{\tau z}$ are the couplings of the local multipolar moment to the bosonic fields in the spin and orbital channels, respectively. The fermionic Kondo couplings are kept fixed. Our main results are as follows:

- In the special case with the spin and orbital bosonic couplings being equal, $g_{\sigma z} = g_{\tau z}$, we identify a critical fixed point that is accessible by the ϵ -expansion. This critical point, marked by the red point in Fig. 2, describes a one-stage transition for the destruction of the SU(4) spin-orbital Kondo effect.
- We find that the anisotropy between these two bosonic couplings is relevant in the RG sense. This implies that the one-stage Kondo-destruction cannot describe the quantum phase transition along a generic trajectory in the phase diagram.
- Moreover, we are able to determine the complete phase diagram asymptotically exactly, as shown in Fig. 2. This is made possible by realizing that all the phase boundaries meet at the equal-bosonic-coupling critical fixed point, near which the run-away RG flows are still small within the ϵ -expansion. It is further substantiated by a more comprehensive RG analysis presented in the SI (Secs. C,D).

The overall phase diagram implies two stages of Kondo-destruction QCPs for *any* generic tuning trajectory at zero temperature, one each in the spin and orbital channels despite their entwining in the Hamiltonian. This is illustrated by the sequence of quantum phase transitions along the solid black lines in Fig. 2.

Model and Solution Methods. We now specify the model and describe the setup for our asymptotically exact analysis. The multipolar Bose-Fermi Kondo model, schematically described by

Fig. 1, is given by the following Hamiltonian:

$$H_{\text{BFK}} = H_0 + H_{\text{K},0} + H_{\text{BK}} . \quad (1)$$

Here, H_0 is the non-interacting part for the conduction electron $c_{p,i\alpha}$ and the bosonic baths $\vec{\phi}_{\kappa}, q$ (where $\kappa = \sigma, \tau, m$):

$$H_0 = \sum_{p,i\alpha} \epsilon_p c_{p,i\alpha}^\dagger c_{p,i\alpha} + \sum_q W_q \left(\vec{\phi}_{\sigma,q}^\dagger \cdot \vec{\phi}_{\sigma,q} + \vec{\phi}_{\tau,q}^\dagger \cdot \vec{\phi}_{\tau,q} + \vec{\phi}_{m,q}^\dagger \cdot \vec{\phi}_{m,q} \right) . \quad (2)$$

To set up controlled RG calculation, we introduce an expansion parameter ϵ , which is defined through the bosonic spectrum W_q :

$$\sum_q [\delta(\omega - W_q) - \delta(\omega + W_q)] = \left(\frac{K_0^2}{\pi} \right) |\omega|^{1-\epsilon} \text{sgn } \omega , \quad (3)$$

with $0 < \epsilon < 1$, and for $|\omega| < \Lambda$, which specifies a high-energy cut-off scale. The fermionic Kondo coupling between the local multipolar moment and conduction electrons is as follows:

$$H_{\text{K},0} = [J_\sigma \vec{\sigma} \cdot \vec{\sigma}_c + J_\tau \vec{\tau} \cdot \vec{\tau}_c + 4J_M (\vec{\sigma}_i \otimes \vec{\tau}) \cdot (\vec{\sigma}_c \otimes \vec{\tau}_c)] , \quad (4)$$

where $\vec{\sigma}$ ($\vec{\tau}$) and $\vec{\sigma}_c$ ($\vec{\tau}_c$) are the spin (orbital) operators of the single impurity and the conduction electrons, respectively. Further details and definitions are given in the Methods (Sec. I).

Finally, the coupling between the local multipolar moment and the bosonic bath is given by:

$$H_{\text{BK}} = g_{\sigma z} \sigma_z \phi_{\sigma z} + g_{\tau z} \tau_z \phi_{\tau z} + g_m (\sigma_z \otimes \tau_z) \phi_m , \quad (5)$$

where $\vec{\phi}_\kappa = \sum_q \left(\vec{\phi}_{\kappa,q} + \vec{\phi}_{\kappa,-q}^\dagger \right)$ with $\kappa = \sigma, \tau, m$. We focus on the Ising-anisotropic case for the couplings in both the spin and orbital channels ($g_{\sigma z}$ and $g_{\tau z}$, respectively) as well as for the spin-orbital mixed coupling (g_m). The BFK model H_{BFK} (Eq. 1) is mapped from a multipolar Kondo lattice model that contains a lattice of local levels with a four-fold degeneracy by the scheme of extended dynamical mean field theory [56–59].

We now summarize how to set up the framework to tackle this rich problem using the (asymptotically exact) RG approach. We aim to determine the generic phase diagram in the $g_{\sigma z}$ - $g_{\tau z}$ parameter space. In other words, we fix the fermionic Kondo couplings and vary $g_{\sigma z}$ and $g_{\tau z}$, and we can keep the mixed bosonic coupling $g_m = 0$ (see the Methods, Sec. I). We are able to set up systematic RG calculations using a Coulomb-gas representation, as described in some detail in the Methods (Sec. I). We achieve this by dividing the analysis into two steps. First, we analyze

the problem along a fine-tuned trajectory in the phase diagram: along the diagonal in the $g_{\sigma z}$ - $g_{\tau z}$ space, viz. the trajectory “I” in Fig. 3(a). This analysis leads to an anchoring point, which allows us to determine the sequence of quantum phase transitions along generic trajectories of the phase diagram.

Quantum phase transitions: fine-tuned case. We now carry out RG calculation of the spin-orbital coupled Bose-Fermi Kondo model (Eq. 1). As outlined in the Methods (Sec. I), we will start from trajectory “I” of Fig. 3(a), which corresponds to the fine-tuned case of equal bosonic couplings in the spin and orbital channels, $g_{\sigma z} = g_{\tau z}$. We demonstrate a critical point [marked by the red solid point in Fig. 3(a)] that is accessible by an ϵ -expansion in our RG analysis. It describes a direct transition from the spin and orbital Kondo-destroyed (KD) phase to the fully (spin or orbital) Kondo-screened (KS) phase. It will be shown in the next section that, by analyzing the vicinity of this critical point, we can determine the structure of the overall phase diagram.

Generally the total number of coupling constants is seven (see the Methods, Sec. I). However, under the trajectory $g_{\sigma z} = g_{\tau z} = g$, some of the coupling constants are irrelevant, or can be combined due to the symmetry constraint, and thus the numbers of relevant RG equations (the beta functions) is substantially reduced. We leave the details in the SI (Sec. D), and present the final reduced beta functions and their analysis in the Methods (Sec. II). The RG beta functions are expressed in terms of $y \propto J_{\sigma\perp} = J_{\tau\perp}$, which flips either spin or orbital indices, $M \propto g_{\sigma z}^2 = g_{\tau z}^2 = g^2$, and $y_1 \propto J_{M1}$, which is the part of the Kondo coupling J_M that flips both the spin and orbital indices (see Eq. S8 in the SI, Sec. C).

From these reduced beta functions, Eq. 7, we identify a critical point marked by the red dot in Fig. 3 and labeled as **R1**. Importantly, this fixed point is accessible by our ϵ -expansion. It has one relevant direction and separates the spin and orbital KD phase from the SU(4) KS phase, which we call **K3** for latter convenience. Because **R1** is accessible by the ϵ -expansion, we can address what happens in the vicinity of this fixed point. We will show in the next section that any small asymmetry between $g_{\tau z}$ and $g_{\sigma z}$ around **R1** is relevant in the RG sense. As a result, the direct phase transition between spin and orbital KD phase and SU(4) KS phase is fine-tuned. In other words, this direct transition occurs at a point in the parameter space – the red dot in Fig. 3(a,b) – instead of through a boundary line.

Quantum phase transitions: generic cases. So far we have considered the case of equal bosonic couplings in the spin and orbital channels, *i.e.*, $g_{\sigma z} = g_{\tau z} = g$. However, these two couplings are generically different. Thus, we have to determine the quantum phase transitions along trajectories

away from the diagonal in the $g_{\sigma z}$ - $g_{\tau z}$ parameter space. We find that there are two sets of trajectories, which are marked by “II” and “III” in Fig. 3(a). We describe our analyses of these two cases in turn.

We next consider the transition between the spin and orbital KD phase and the spin or orbital KS phase. Importantly, we do so by starting from the RG trajectory around the critical point **R1** where $g_{\sigma z} = g_{\tau z} = g^*$ between the spin and orbital KD and the SU(4) KS phases. As we have just alluded to, around **R1**, any small asymmetry between $g_{\tau z}$ and $g_{\sigma z}$ is relevant with the scaling dimension $\sqrt{2\epsilon}$ (up to the order $\sqrt{\epsilon}$) in RG sense,.

Consider first the case with a slight increase of the coupling constant $g_{\tau z}$, while keeping all the other parameters fixed; in other words, now $g_{\tau z} > g_{\sigma z} = g^*$. The RG trajectory will flow towards $g_{\tau z} \rightarrow \infty$. We can then vary $g_{\sigma z}$ to map out the RG flow. The corresponding trajectory in the phase diagram are denoted as arrow (II) in Fig. 3(a). Along this trajectory, the reduced beta functions are determined (see the Methods, Eq. 8) in terms of $y_2 \propto J_{\sigma\perp}$, which flips only the orbital indices, and $M^\sigma \propto g_{\sigma z}^2$.

From the reduced beta functions (Eq. 8), one can identify another critical fixed point $(y_2^*, M^{\sigma*}) = \left(\frac{\sqrt{\epsilon}}{2}, 1\right)$. This fixed point has one relevant direction with scaling dimension $\sqrt{2\epsilon}$ (up to the order $\sqrt{\epsilon}$) and separates the spin KS phase ($y_2 \rightarrow \infty, M^\sigma \rightarrow 0$) from the spin and orbital KD phase ($y_2 \rightarrow 0, M^\sigma \rightarrow \infty$).

The schematic RG flow structure is shown in Fig. 4, where the spin and orbital KD phase and the spin KS phase, denoted as **G** and **K1**, respectively, are separated by the critical point denoted as **F1**. Based on this RG structure, we establish the transition between the spin and orbital KD phase and the spin KS phase. By applying a precisely parallel analysis, we establish the phase transition between spin and orbital KD phase and the orbital KS phase; we name the associated critical point as **F2**.

We have so far analyzed the transitions out of the spin and orbital KD phase. This phase can transit into the spin or orbital KS phase without fine-tuning the parameters. It can also transit into the SU(4) KS phase by fine-tuning the parameters.

Because the spin or orbital KS phase and the SU(4) KS phase correspond to different stable strong coupling fixed points, there must be other generic critical points that separate them. These generic critical points describe the phase transition between the spin or orbital KS phase and the SU(4) KS phase, as shown in the phase diagram trajectory denoted as the dashed arrow (III) in Fig. 3(a). Here we would like to finally establish the transition between the spin or orbital KS

phase and the SU(4) KS phase, which corresponds to the trajectories (III) in Fig. 3(a).

Again, we focus on the RG trajectory around the critical point **R1** where $g_{\sigma z} = g_{\tau z} = g^*$ between the spin and orbital KD and SU(4) KS phases. If we keep all the other parameters fixed but just slightly decrease the coupling constant $g_{\sigma z}$, that is, $g_{\sigma z} < g_{\tau z} = g^*$, then the RG trajectory will flow towards $g_{\sigma z} \rightarrow 0$. We can then vary $g_{\tau z}$ to explore the RG trajectory. The corresponding trajectories in the phase diagram are denoted as the arrow III in Fig. 3(a).

However, unlike **R1** and **F1**, the real locations of the **X1** is harder to identify directly from the beta functions. To proceed, we exploit the property of the critical point **R1** that we alluded to earlier: Here, all of the fugacity y is $\sim \sqrt{\epsilon}$ around **R1**. Near **R1**, one can thus neglect in a controlled way the higher order terms of $\sqrt{\epsilon}$ in the beta functions of the fugacity (See the SI, Sec. D for more details), and in the end the reduced beta functions are determined (see the Methods, Eq. 9) in terms of y_1 , M^τ and $y_3 \propto J_{\tau\perp}$.

From the reduced beta functions (Eq. 9), we identify a critical line $(y_1^*, y_3^*, M^{\tau*}) = \left(a, \frac{\sqrt{\epsilon - 4a^2}}{2}, 1\right)$ where a is a constant, which separates the spin and orbital KS phase from the spin KS phase and corresponds to the critical point **X1** in Fig. 5 with scaling dimension $\sqrt{2\epsilon}$. By a parallel analysis, the transition between the spin and orbital KS phase and the orbital KS phase can also be established.

Phase diagram and the sequential Kondo destruction. Based on the above, we have established the overall phase diagram, which is shown in Fig. 2. This phase diagram is also seen through a complete RG flow, Fig. 3(a), which combines the RG flows along the various trajectories we have described in the previous sections. (A complementary, and more comprehensive, way of deriving this complete RG flow is given in the SI, Sec. D.) We summarize the characterization of the various phases and their transitions as follows:

- The boxes **K1-K3** are different kinds of strong Kondo coupling fixed points, and the box **G** is the spin and orbital KD fixed point. These fixed points are all stable according to the beta functions (Eq. S44), and thus describe phases of matter.
- The red box **R1** is a multi-critical point between the spin and orbital KD phase and SU(4) KS phase since there are two relevant directions around it.
- The blue boxed **F1-F2** are generic critical point separating different types the spin and orbital KD phases to either spin or orbital KS phases.

- Because the strong Kondo coupling fixed points **K1**, **K2**, and **K1** are stable fixed points, they are separated by the generic critical points **X1** and **X2**. The generic critical points **X1** and **X2** control the critical phenomena of the trajectories III in Fig. 3(a).

The solid black arrows in Fig. 2 marks the generic tuning trajectories in the zero-temperature phase diagram. Along each of such trajectories, two-stages of Kondo destruction take place, each characterizing a QCP in the spin or orbital channel. This asymptotically exact result provides a firm theoretical basis to understand the field-induced quantum phase transitions that have been experimentally observed in $\text{Ce}_3\text{Pd}_{20}\text{Si}_6$ [52].

Discussion

In this work, we have performed a detailed renormalization-group analysis of a spin-orbital-entwined Bose-Fermi-Kondo model, which is mapped from a multipolar Kondo lattice model. We are able to determine the overall phase diagram at zero temperature, which reveals the mechanism for the sequential Kondo destruction and shows that it appears for any generic trajectory in the phase diagram. As such, our results provide a firm theoretical basis for understanding the surprising experimental results in the heavy fermion metal $\text{Ce}_3\text{Pd}_{20}\text{Si}_6$ [52]. More generally, our work elucidates the quantum criticality in spin-orbital-coupled heavy fermion systems.

Our asymptotically exact theoretical results also make it clear how the entwining of spins, orbitals and other quantum numbers in local degrees of freedom allows for new types of quantum criticality and associated strange metallicity. This represents a design principle for creating and realizing new forms of quantum criticality and associated strange metallicity: The cooperation of strong correlations, large spin-orbit coupling and crystalline symmetry represents a robust means to create varied local degrees of freedom; and the tuning of such strongly correlated systems can realize a sequence of beyond-Landau quantum critical points. Beyond heavy fermion metals, effective local degrees of freedom have also been advanced for pertinent molecular orbitals of d -electron-based flat band systems [38–41] and moiré states of twisted structures [42–44]. Thus, we expect this design procedure to operate not only in multipolar heavy fermion metals, but also in transition-metal compounds, synthetic systems such as moiré structures and beyond.

Note added. The sequential Kondo destruction that we identify in the minimal prototype multipolar model has now also been seen in a related model that contains additional couplings and has continuous spin symmetry (S. E. Han, D. J. Schultz and Y. B. Kim, “Microscopic theory of multi-stage Fermi surface reconstruction in higher-rank moment quantum materials”).

Methods

I. Model and the Renormalization-Group Method. In the definition of the model, Eqs. 1-4, the spin and orbital operators of the conduction electrons are defined as:

$$\begin{aligned}
 \vec{\sigma}_c &= \frac{1}{2} \sum_{i,\alpha\beta} c_{i\alpha}^\dagger \vec{s}_{\alpha\beta} c_{i\beta} , \\
 \vec{\tau}_c &= \frac{1}{2} \sum_{ij,\alpha} c_{i\alpha}^\dagger \vec{t}_{ij} c_{j\alpha} , \\
 \vec{\sigma} \otimes \vec{\tau}_c &= \frac{1}{4} \sum_{ij,\alpha\beta} c_{i\alpha}^\dagger \vec{s}_{\alpha\beta} \otimes \vec{t}_{ij} c_{j\beta} .
 \end{aligned} \tag{6}$$

Here, we use α, β and i, j to denote the spin and orbital indices, respectively. Thus, $\vec{s}_{\alpha\beta}$ and \vec{t}_{ij} are Pauli matrices in the spin and orbital subspaces, respectively. For the fermionic Kondo Hamiltonian alone, the anisotropy in the couplings is generically unimportant as the system restores the SU(4) symmetry in the Kondo-entangled ground state [8]. We have therefore chosen the bare Kondo Hamiltonian to be SU(2) symmetric in the spin as well as in the orbital sector, with an overall SU(2)⊗SU(2) symmetry. The full renormalized Kondo Hamiltonian (Eq. S8) for the later RG analysis is shown in the SI, Sec. C.

We now describe the framework to tackle this rich problem using the (asymptotically exact) RG approach. Further details can be found in the the SI (Sec. C).

First, our goal is to study the generic phase diagram in the $g_{\sigma z}$ - $g_{\tau z}$ parameter space. In other words, we fix the fermionic Kondo couplings and vary $g_{\sigma z}$ and $g_{\tau z}$. For this purpose, it suffices to keep the mixed bosonic coupling $g_m = 0$. A non-vanishing but small g_m does not modify the structure of the phase diagram, as we show in the SI (Sec. E). To proceed, we use a bosonization approach to represent the BFK model (Eq. 1) in terms of a Coulomb gas, from which a controlled RG calculation based on an expansion in ϵ is possible[60–62]. We note that the Coulomb-gas RG calculation is based on a dilute-instanton expansion, which is non-perturbative in stiffness constants but perturbative in terms of fugacities [60].

Second, the Ising couplings of H_{BK} (Eq. 5) break not only the SU(4) symmetry but also the smaller SU(2)×SU(2) symmetry. While the Kondo couplings in H_K respect the SU(2)×SU(2) symmetry, under the RG flow these couplings will generically become spin anisotropic. It turns out that one needs to consider five types of Kondo couplings. Together with the spin and orbital Ising couplings $g_{\sigma z}$ and $g_{\tau z}$ of H_{BK} (Eq. 5), the total number of RG coupling constants is seven. The large number of the RG charges makes it a challenge to determine the overall RG flow structure.

We are able to accomplish this goal by analyzing the problem in several steps.

Crucially, we take the first step to be a fine-tuned trajectory in the phase diagram. Recall that the $g_{\sigma z}-g_{\tau z}$ parameter space is of our interest. For clarity, we visualize this parameter space in Fig. 3(a), which marks the relevant phases. The fine-tuned trajectory we focus our initial analysis on corresponds to identical couplings to the bosonic baths in the spin and orbital sectors. It goes along the diagonal in the $g_{\sigma z}-g_{\tau z}$ space, and is marked as trajectory ‘‘I’’. The result of the analysis on this fine-tuned trajectory provides an anchoring point, which allows us to determine the sequence of quantum phase transitions along generic trajectories of the phase diagram.

We note that it is possible to rigorously establish the phase diagram, Fig. 3(a), through a comprehensive RG analysis without taking the fine-tuned trajectory ‘‘I’’ as the starting anchoring point. This is described in the SI (Secs. C,D). We choose to present the step-by-step analysis here in the main text, given that it reveals the underlying physics in a considerably more transparent way.

II. RG equations and analysis: fine-tuned case. The RG analysis, described in the SI (Sec. D), leads to the following reduced beta functions:

$$\begin{aligned}\frac{dy_1}{dl} &= (1 - 2M) y_1 + 2y^2, \\ \frac{dy}{dl} &= (1 - M) y + 2y_1 y, \\ \frac{dM}{dl} &= (\epsilon - 4y_1^2 - 4y^2) M.\end{aligned}\tag{7}$$

Note that we can set $J_{\sigma\perp} = J_{\tau\perp}$, given that we are considering a path in the parameter space that preserves the symmetry $\sigma \leftrightarrow \tau$. From these reduced beta functions (Eq. 7), we identify a critical point (up to the order $\sqrt{\epsilon}$) at $(y_1^*, y^*, M^*) = \left(\frac{-1+\sqrt{1+12\epsilon}}{12}, \frac{\sqrt{-1+12\epsilon+\sqrt{1+12\epsilon}}}{6\sqrt{2}}, \frac{5+\sqrt{1+12\epsilon}}{6} \right) \cong \left(0, \frac{\sqrt{\epsilon}}{2}, 1 \right)$. This fixed point has one relevant direction with the scaling dimension $\sqrt{2\epsilon}$ and separates the spin and orbital KD phase ($y_1 \rightarrow 0, y \rightarrow 0, M \rightarrow \infty$) from the SU(4) KS phase ($y_1 \rightarrow \infty, y \rightarrow \infty, M \rightarrow 0$)[64]. The RG flow structure of the reduced beta functions (Eq. 7) is plotted in Fig. 3. For latter convenience, we name SU(4) KS phase as **K3**, and the critical point (the red dot in Fig. 3) as **R1**.

For our analysis, one feature of the fixed point **R1** plays a crucial role. While the fixed-point value for the RG charge M is $O(1)$, the values for the RG charges (the fugacities) y_1 and y are of order $\sqrt{\epsilon}$. Because of this feature, the quadratic-in- y_α terms in the beta-functions of the fugacities turn out to be unimportant for both RG flow structure and the leading order of the scaling dimensions. The same conclusion is also seen in the scaling dimensions of the RG variables near **R1**; to

the leading non-vanishing order in ϵ , they are the same regardless of whether the quadratic-in- y_α terms are kept in the beta-functions of the fugacities. In the next section, we'll see how this allows us to determine the overall structure of the phase diagram by expanding the RG equations around the fixed point **R1**. In particular, it allows us to carry out a complete analysis of the quantum phase transition along trajectory "III", which otherwise would have been much harder to achieve.

III. RG equations for the generic case – trajectory II. Along this trajectory, the reduced beta functions are calculated to be as follows:

$$\begin{aligned}\frac{dy_2}{dl} &= (1 - M^\sigma) y_2 , \\ \frac{dM^\sigma}{dl} &= (\epsilon - 4y_2^2) M^\sigma .\end{aligned}\tag{8}$$

Again, we leave the details of the derivation to the SI (Sec. D).

IV. RG equations for the generic case – trajectory III. Along this trajectory, the reduced beta functions are as follows:

$$\begin{aligned}\frac{dy_1}{dl} &= (1 - M^\tau) y_1 , \\ \frac{dy_3}{dl} &= (1 - M^\tau) y_3 , \\ \frac{dM^\tau}{dl} &= (\epsilon - 4y_1^2 - 4y_3^2) M^\tau .\end{aligned}\tag{9}$$

-
- [1] B. Keimer and J. E. Moore, *The physics of quantum materials*, Nat. Phys. **13**, 1045 (2017).
- [2] S. Paschen and Q. Si, *Quantum phases driven by strong correlations*, Nat. Rev. Phys. **3**, 9-26 (2021).
- [3] H. Hu, L. Chen, and Q. Si, *Quantum critical metals: Dynamical Planckian scaling and loss of quasi-particles*, arXiv:2210.14183 (2022).
- [4] P. W. Phillips, N. E. Hussey, and P. Abbamonte, *Stranger than metals*, Science **377**, eabh4273 (2022).
- [5] G. R. Stewart, *Non-Fermi-liquid behavior in d- and f-electron metals*, Rev. Mod. Phys. **73**, 797-855 (2001).
- [6] P. Coleman and A. J. Schofield, *Quantum Criticality*, Nature **433**, 226-229 (2005).
- [7] S. Kirchner, S. Paschen, Q. Y. Chen, S. Wirth, D. L. Feng, J. D. Thompson, and Q. Si, *Colloquium: Heavy-electron quantum criticality and single-particle spectroscopy*, Rev. Mod. Phys. **92**, 011002 (2020).
- [8] A. C. Hewson *The Kondo Problem to Heavy Fermions*, Cambridge Studies in Magnetism (Cambridge Univ. Press, 1993).
- [9] Q. Si, S. Rabello, K. Ingersent, and J. Smith *Locally critical quantum phase transitions in strongly correlated metals*, Nature **413**, 804-808 (2001).
- [10] P. Coleman, C. Pépin, C., Q. Si, and R. Ramazashvili, *How do Fermi liquids get heavy and die?* J. Phys. Condens. Matter **13**, R723-R738 (2001).
- [11] T. Senthil, M. Vojta, and S. Sachdev, *Weak magnetism and non-Fermi liquids near heavy-fermion critical points*, Phys. Rev. B **69**, 035111 (2004).
- [12] A. Schröder, G. Aeppli, R. Coldea, M. Adams, O. Stockert, H. v. Löhneysen, E. Bucher, R. Ramazashvili, and P. Coleman, *Onset of antiferromagnetism in heavy-fermion metals*, Nature **407**, 351 (2000).
- [13] S. Paschen, T. Lühmann, S. Wirth, P. Gegenwart, O. Trovarelli, C. Geibel, F. Steglich, P. Coleman, and Q. Si, *Hall-effect evolution across a heavy-fermion quantum critical point*, Nature **432**, 881 (2004).
- [14] H. Shishido, R. Settai, H. Harima, and Y. Onuki, *A drastic change of the Fermi surface at a critical pressure in CeRhIn₅: dHvA study under pressure*, J. Phys. Soc. Jpn. **74**, 1103 (2005).
- [15] T. Park, V. A. Sidorov, F. Ronning, J.-X. Zhu, Y. Tokiwa, H. Lee, E. D. Bauer, R. Movshovich, J. L. Sarrao, and J. D. Thompson, *Isotropic quantum scattering and unconventional superconductivity*, Nature **456**, 366 (2008).
- [16] L. Prochaska, X. Li, D. C. MacFarland, A. M. Andrews, M. Bonta, E. F. Bianco, S. Yazdi, W. Schrenk,

- H. Detz, A. Limbeck, Q. Si, E. Ringe, G. Strasser, J. Kono, and S. Paschen, *Singular charge fluctuations at a magnetic quantum critical point*, *Science* **367**, 285 (2020).
- [17] D. H. Nguyen, A. Sidorenko, M. Taupin, G. Knebel, G. Lapertot, E. Schuberth, and S. Paschen, *Superconductivity in an extreme strange metal*, *Nat. Commun.* **12**, 4341 (2021).
- [18] A. Patri, I. Khait, and Y. B. Kim, *Emergent non-Fermi-liquid phenomena in multipolar quantum impurity systems*, *Phys. Rev. Research* **2**, 013257 (2020).
- [19] A. Patri, and Y. B. Kim, *Critical Theory of Non-Fermi Liquid Fixed Point in Multipolar Kondo Problem*, *Phys. Rev. X* **10**, 041021 (2020).
- [20] H.-H. Lai, E. Nica, W.-J. Hu, S.-S. Gong, S. Paschen, and Q. Si, *Kondo Destruction and Multipolar Order—Implications for Heavy Fermion Quantum Criticality*, arXiv:1807.09258.
- [21] J. S. Van Dyke, G. H. Zhang, and R. Flint, *Field-induced ferrohastatic phase in cubic non-Kramers doublet systems*, *Phys. Rev. B* **100**, 205122 (2019).
- [22] G. H. Zhang, J. S. Van Dyke, and R. Flint *Cubic hastatic order in the two-channel Kondo-Heisenberg model*, *Phys. Rev. B* **98**, 235143 (2018).
- [23] C. J. Bolech and N. Andrei, *Solution of the multichannel Anderson impurity model: Ground state and thermodynamics*, *Phys. Rev. B* **71**, 205104 (2005).
- [24] C. J. Bolech and N. Andrei *Solution of the Two-Channel Anderson Impurity Model: Implications for the Heavy Fermion UBe_{13}* , *Phys. Rev. Lett.* **88**, 237206 (2002).
- [25] D. L. Cox and A. Zawadowski, *Exotic Kondo Effects in Metals: Magnetic Ions in a Crystalline Electric Field and Tunnelling Centres*, *Adv. Phys.* **47**, 599 (1998).
- [26] Q. Si, R. Yu, and E. Abrahams, *High-temperature superconductivity in iron pnictides and chalcogenides*, *Nat. Rev. Mater.* **1**, 16017 (2016).
- [27] C. Aron, and G. Kotliar, *Analytic theory of Hund's metals: a renormalization group perspective*, *Phys. Rev. B* **91**, 041110 (2015).
- [28] E. Walter, K. Stadler, S.-S. B. Lee, Wang, G. Kotliar, A. Weichselbaum, and J. von Delf, *Uncovering Non-Fermi-Liquid Behavior in Hund Metals: Conformal Field Theory Analysis of an $SU(2)\times SU(3)$ Spin-Orbital Kondo Model*, *Phys. Rev. X* **10**, 031052 (2020).
- [29] T. T. Ong and P. Coleman, *Local Quantum Criticality of an Iron-Pnictide Tetrahedron*, *Phys. Rev. Lett.* **108**, 107201 (2012).
- [30] Y. Nishida, *$SU(3)$ Orbital Kondo Effect with Ultracold Atoms*, *Phys. Rev. Lett.* **111**, 135301 (2013).
- [31] K. Le Hur, and P. Simon, *Smearing of charge fluctuations in a grain by spin-flip assisted tunneling* ,

- Phys. Rev. B **67**, 201308 (2003).
- [32] R. M. Potok, I. G. Rau, H. Shtrikman, Y. Oreg, and D. Goldhaber-Gordon, *Observation of the two-channel Kondo effect*, Nature **446**, 167-171 (2007).
- [33] A. Mitchell, A. Liberman, E. Sela, and I. Affleck *SO(5) non-Fermi liquid in a Coulomb box device*, Phys. Rev. Lett. **126**, 147702 (2021).
- [34] A. Horvat, R. Zitko, and J. Mravlje, *Low-energy physics of three-orbital impurity model with Kanamori interaction*, Phys. Rev. B **94**, 165140 (2016).
- [35] J. G. Rau and H.-Y. Kee, *Symmetry breaking via hybridization with conduction electrons in frustrated Kondo lattices*, Phys. Rev. B **89**, 075128 (2014).
- [36] P. Coleman, L. B. Ioffe, and A. M. Tsvelik, *Simple formulation of the two-channel Kondo model*, Phys. Rev. B **52**, 6611 (1995).
- [37] I. Affleck and A. W. W Ludwig, *Critical theory of overscreened Kondo fixed points*, Nucl. Phys. B **360**, 641(1991).
- [38] L. Ye, S. Fang, M. G. Kang, J. Kaufmann, Y. Lee, J. Denlinger, C. Jozwiak, A. Bostwick, E. Rotenberg, E. Kaxiras, D. C. Bell, O. Janson, R. Comin, and J. G. Checkelsky, *A flat band-induced correlated kagome metal*, arXiv:2106.10824.
- [39] S. A. Ekahana, Y. Soh, A. Tamai, D. Gosálbez-Martínez, M. Yao, A. Hunter, W. Fan, Y. Wang, J. Li, A. Kleibert, C. A. F. Vaz, J. Ma, Y. Xiong, O. V. Yazyev, F. Baumberger, M. Shi, and G. Aeppli, *Anomalous quasiparticles in the zone center electron pocket of the kagomé ferromagnet Fe₃Sn₂*, arXiv:2206.13750.
- [40] H. Hu and Q. Si, *Coupled topological flat and wide bands: Quasiparticle formation and destruction*, arXiv:2209.10396.
- [41] L. Chen, F. Xie, S. Sur, H. Hu, S. Paschen, J. Cano, and Q. Si, *Emergent flat band and topological Kondo semimetal driven by orbital-selective correlations*, arXiv:2212.08017.
- [42] A. Ramires and J. L. Lado, *Emulating heavy fermions in twisted trilayer graphene*, Phys. Rev. Lett. **127**, 026401 (2021).
- [43] Z.-D. Song and B. A. Bernevig, *Magic-angle twisted bilayer graphene as a topological heavy fermion problem*, Phys. Rev. Lett. **129**, 047601 (2022).
- [44] D. Guerzi, J. Wang, J. Zang, J. Cano, J. H. Pixley, and A. Millis, *Chiral Kondo lattice in doped MoTe₂/WSe₂ bilayers*, arXiv:2207.06476.
- [45] S. Paschen and J. J. Larrea, *Ordered Phases and Quantum Criticality in Cubic Heavy Fermion Com-*

- pounds, J. Phys. Soc. Jpn **83**, 061004 (2014).
- [46] A. Sakai and S. Nakatsuji *Kondo effects and multipolar order in the cubic PrTr₂Al₂₀ (Tr=Ti, V)*, J. Phys. Soc. Jpn. **80**, 063701 (2011).
- [47] Y. Shimura, M. Tsujimoto, B. Zeng, L. Balicas, A. Sakai, and S. Nakatsuji, *Field-induced quadrupolar quantum criticality in PrV₂Al₂₀*, Phys. Rev. B **91**, 241102(R) (2015).
- [48] A. McCollam, B. Andraka, S. R. Julian, *Fermi volume as a probe of hidden order*, Phys. Rev. B **88**, 075102 (2013).
- [49] E. D. Bauer, N. A. Frederick, P. C. Ho, V. S. Zapf, M. B. Maple, *Superconductivity and heavy fermion behavior in PrOs₄Sb₁₂*, Phys. Rev. B **65**, 100506 (2002).
- [50] E. W. Rosenberg, J.-H. Chu, J. P. C. Ruff, A. T. Hristov, and I. R. Fisher, *Divergence of the quadrupole-strain susceptibility of the electronic nematic system YbRu₂Ge₂*, Proc. Natl. Acad. Sci. U.S.A **116**, 7232-7237 (2019).
- [51] H. S. Jeevan, C. Geibel, and Z. Hossain, *Quasi-quartet crystal-electric-field ground state with possible quadrupolar ordering in the tetragonal compound YbRu₂Ge₂*, Phys Rev B **73**, 020407 (2006).
- [52] V. Martelli, A. Cai, E. M. Nica, M. Taupin, A. Prokofiev, C.-C. Liu, H.-H. Lai, R. Yu, K. Ingersent, R. K \ddot{a} chler, A. M. Strydom, D. Geiger, J. Haenel, J. Larrea, Q. Si, and S. Paschen *Sequential localization of a complex electron fluid*, Proc. Natl. Acad. Sci. U.S.A **116**, 17701 (2019).
- [53] J. Custers, K. Lorenzer, M. M \ddot{a} ller, A. Prokofiev, A. Sidorenko, H. Winkler, A. M. Strydom, Y. Shimura, T. Sakakibara, R. Yu, Q. Si, and S. Paschen *Destruction of the Kondo effect in the cubic heavy-fermion compound Ce₃Pd₂₀Si₆*, Nature Materials **11**, 189 (2012).
- [54] R. Shiina, H. Shiba, and P. Thalmeier, *Magnetic-Field Effects on Quadrupolar Ordering in a Γ_8 -Quartet System CeB₆*, J. Phys. Soc. Jpn. **66**, 1741 (1997).
- [55] K.-A. Lorenzer, *Quantum critical behaviour in cubic heavy-fermion compounds*, PhD thesis, Vienna University of Technology, (2012).
- [56] H. Hu, L. Chen, and Q. Si, *Extended Dynamical Mean Field Theory for Correlated Electron Models*, arXiv:2210.14197 (2022).
- [57] Q. Si and J. L. Smith, *Kosterlitz-Thouless Transition and Short Range Spatial Correlations in an Extended Hubbard Model*, Phys. Rev. Lett. **77**, 3391 (1996).
- [58] J. Smith and Q. Si, *Spatial correlations in dynamical mean-field theory*, Phys. Rev. B **61**, 5184 (2000).
- [59] R. Chitra and G. Kotliar, *Effective-action approach to strongly correlated fermion systems*, Phys. Rev. B **63**, 115110 (2001).

- [60] L. Zhu, and Q. Si, *Critical local-moment fluctuations in the bose-fermi kondo model*, Phys. Rev. Lett. **66**, 024426 (2002).
- [61] Q. Si and J. Smith, *Kosterlitz-Thouless Transition and Short Range Spatial Correlations in an Extended Hubbard Model*, Phys. Rev. Lett. **77**, 3391 (1996).
- [62] J. Smith and Q. Si, *Non-Fermi liquids in the two-band extended Hubbard model*, Europhys. Lett. **45**, 228 (1999).
- [63] J. Smith, *Non-Fermi liquid states in strongly correlated electron systems*, PhD Thesis (2000).
- [64] Here we ignore a unstable fixed point $(y_1^*, y^*, M^*) = \left(\frac{\sqrt{\epsilon}}{2}, 0, \frac{1}{2}\right)$; because the RG trajectories around it can flow toward the generic critical point $\left(0, \frac{\sqrt{\epsilon}}{2}, 1\right)$, it does not influence the structure of the RG flow diagram (Fig. 3).
- [65] S. Chakravarty and J. E. Hirsch, *Approximate mapping of the two-impurity symmetric Anderson model in the local-moment regime to a classical problem*, Phys. Rev. B **25**, 3273 (1982).
- [66] A. O. Caldeira and A. J. Leggett, *Quantum tunnelling in a dissipative system*, Ann. Phys. (N.Y.) **149**, 374 (1983).
- [67] J. Cardy, *One-dimensional models with $1/r^2$ interactions*, J. Phys. A: Math. Gen. **14**, 1407 (1981).
- [68] Q. Si and G. Kotliar, *Metallic non-Fermi-liquid phases of an extended Hubbard model in infinite dimensions*, Phys. Rev. B **48**, 13881 (1993).

Acknowledgments

We thank Ang Cai, Kevin Ingersent, Emilian Nica and Rong Yu for useful discussions. The work has been supported in part by the NSF Grant No. DMR-2220603 and the Robert A. Welch Foundation Grant No. C-1411. Work in Vienna has been supported by the Austrian Science Fund (P29296 and 29279) and the European Community (H2020 Project No. 824109). One of us (Q.S.) acknowledges the hospitality of the Aspen Center for Physics, which is supported by the NSF grant No. PHY-1607611.

Author contributions

C.-C. L., S. P. and Q.S. conceived the research. C.-C. Liu and Q.S. carried out theoretical model studies. S. P. and Q. S. provided insights into multipolar heavy fermion systems. C.-C. L. and Q. S. wrote the manuscript, with input from S.P..

Competing interests

The authors declare no competing interests.

Additional information

Correspondence and requests for materials should be addressed to Q.S. (qmsi@rice.edu)

Data availability

All data needed to evaluate the conclusions in the paper are presented in the paper and/or the Supplementary Information.

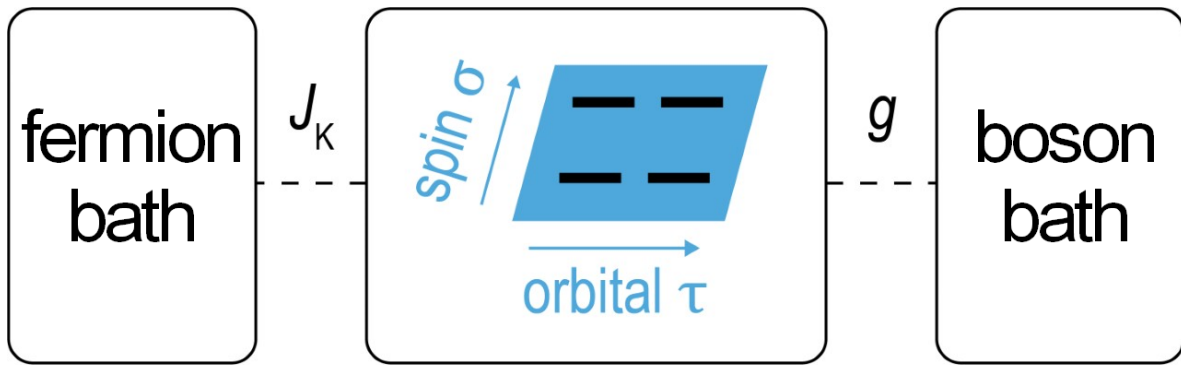


FIG. 1. **Illustration of the model.** The multipolar Bose-Fermi Kondo model (Eq. 1) describes entwined local spin-orbital degrees of freedom that are coupled to a bosonic and fermionic bath.

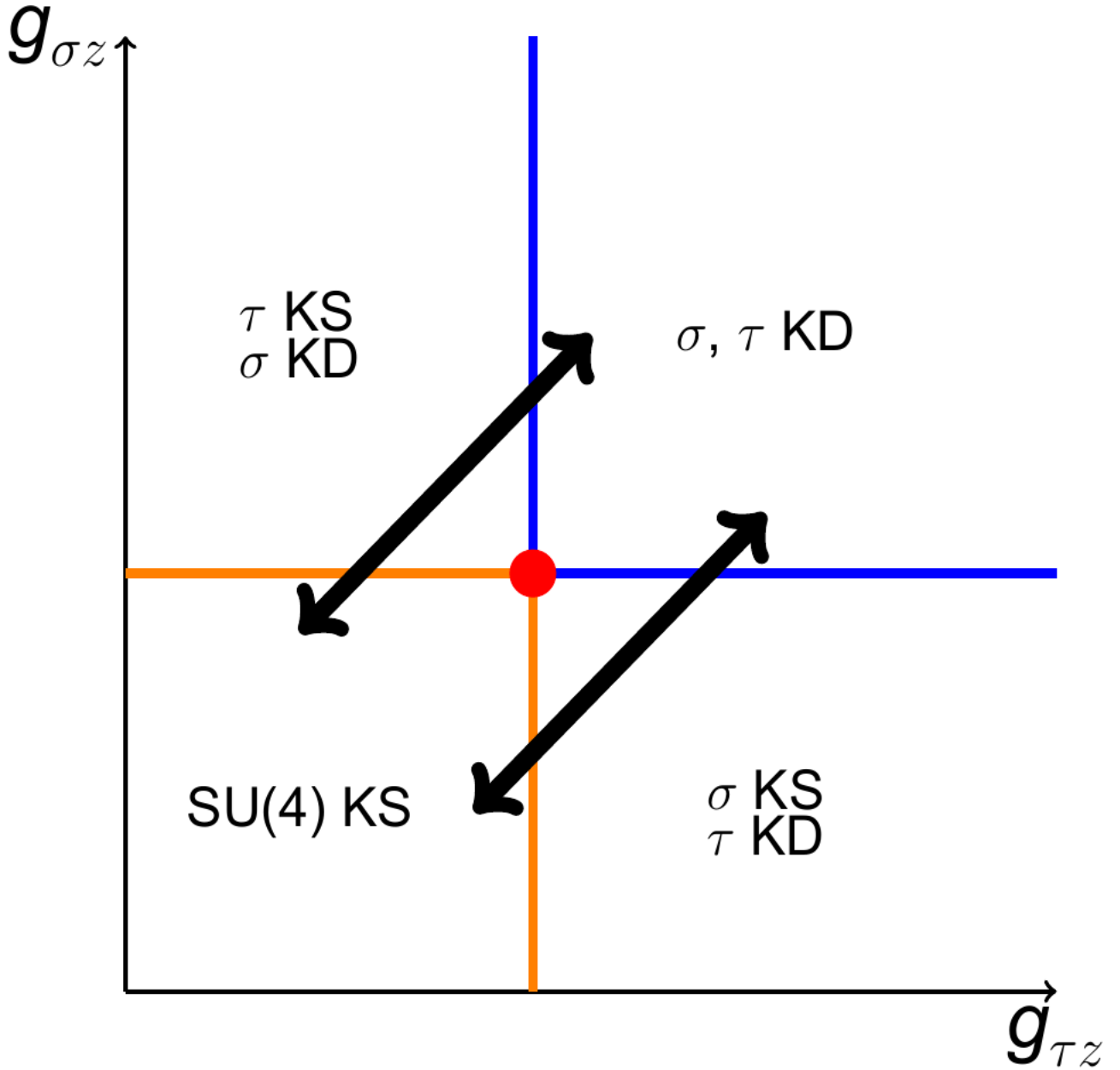


FIG. 2. **The overall phase diagram.** Presented here is the phase diagram in the $g_{\sigma z}$ - $g_{\tau z}$ parameter space, for fixed Kondo couplings, of the model given in Eq. 1. KD and KS refer to the phases with Kondo-destruction and Kondo screening, respectively, whereas σ and τ refer to spin and orbital (c.f. Fig. 1), respectively. The black arrows mark generic trajectories in the parameter space that correspond to the tuning of a non-thermal physical control parameter. The overall phase diagram implies two-stages of Kondo destruction along any generic tuning trajectory.

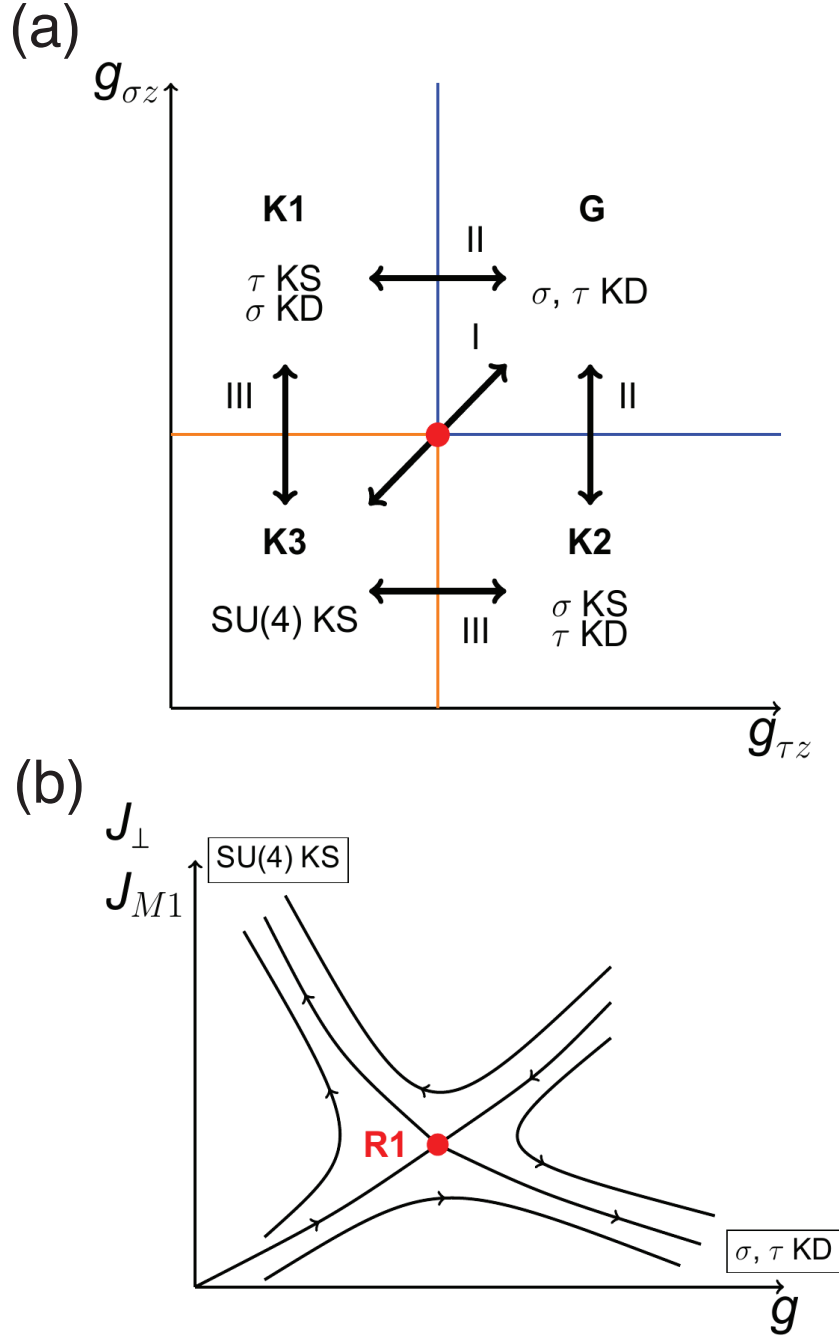


FIG. 3. **Renormalization-group analysis.** (a) Trajectories in the parameter space of the BFK model (Eq. 1), marked as “I”-“III”, along which the RG analyses are carried out in steps. The labels “G”, “K1”, “K2” and “K3” describe the RG fixed points for the corresponding phases. (b) RG flow diagram of the reduced beta functions (Eq. 7), where $g = g_{\sigma z} = g_{\tau z}$. “R1” marks the unstable fixed point that captures the transition along the fine-tuned trajectory “I” of (a).

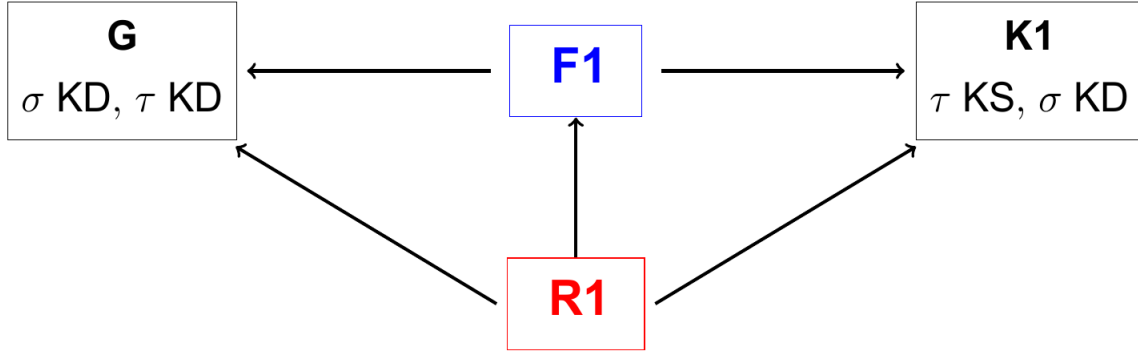


FIG. 4. **The schematic renormalization-group flow structure.** Illustrated here is the RG flow structure of the phase transition between the orbital and spin KD phase and the spin KS phase denoted as **G** and **K1**, respectively. Around the multi-critical point **R1**, once the $g_{\sigma z}$ is slightly enlarged, the RG trajectory will flow toward **F1**, which is the generic critical point separating **G** and **K1**.

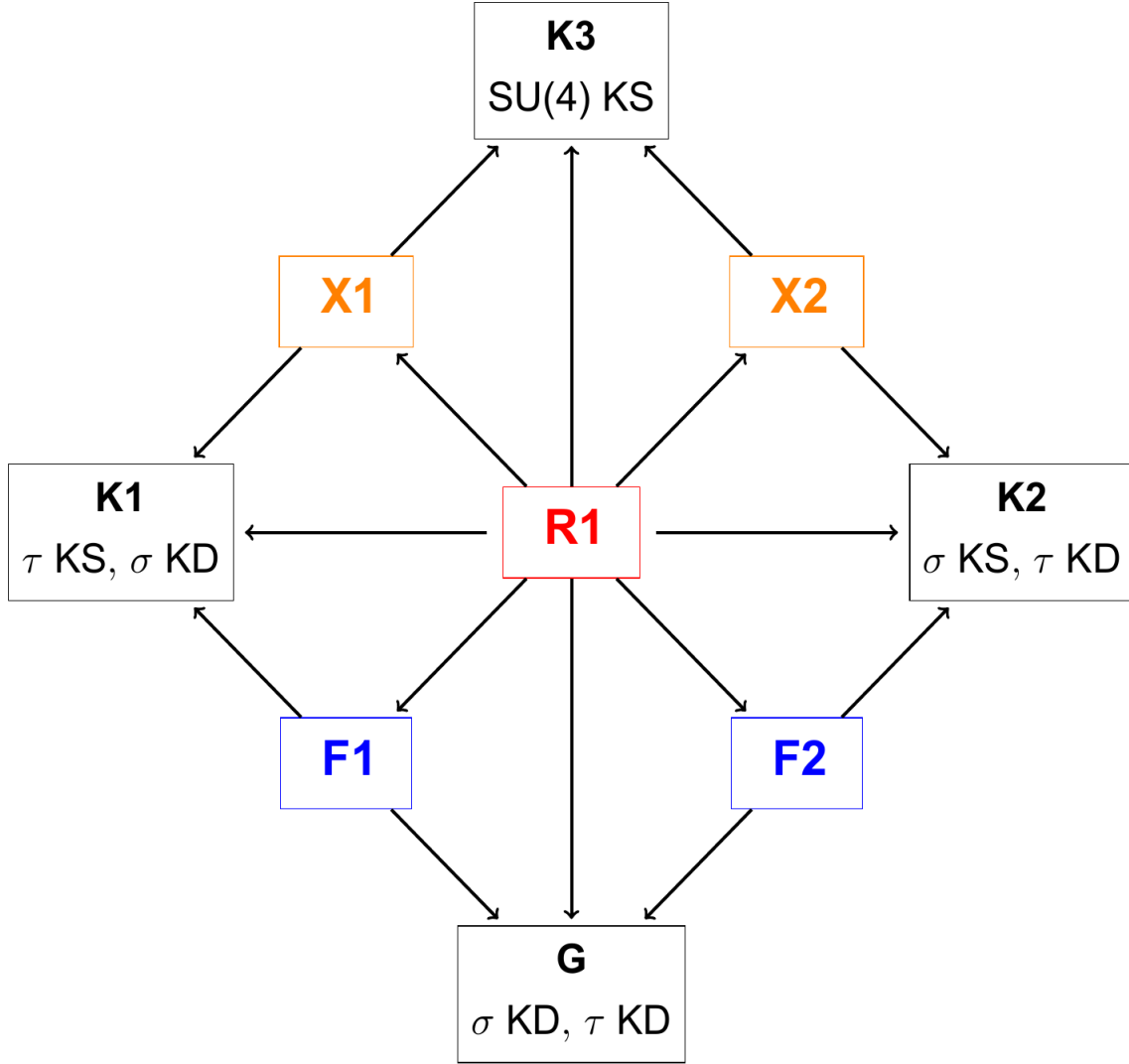


FIG. 5. **The schematic structure of the fixed points.** Illustrated here are the structure of the fixed points and the relative RG flow of the BFK model (Eq. 1), as derived from the RG analysis. KS and KD denote the Kondo-screened and Kondo-destroyed fixed points, respectively. The boxes **K1-K3** are different kinds of strong Kondo coupling fixed points, and the box **G** is the spin and orbital KD fixed point. The red box **R1** is a multi-critical point between spin and orbital KD phase and SU(4) KS phase. The blue boxed **F1-F2** are generic critical point separating different types the spin and orbital KD phases to either spin or orbital KS phases. Because the strong Kondo coupling fixed points **K1**, **K2**, and **K3** are stable fixed points, they are separated by the generic critical points, denoted as orange boxes **X1** and **X2**.

Supplementary Information

A. The case of $\text{Ce}_3\text{Pd}_{20}\text{Si}_6$

In $\text{Ce}_3\text{Pd}_{20}\text{Si}_6$, every Ce^{3+} ion contributes one localized 4f electron. Because of the strong spin-orbit coupling, the spin and orbital degree of freedom of the 4f electron are coupled together into a total angular momentum $J = 5/2$ state that has six-fold degeneracy and hence supports not only dipole moment but also higher-order multipolar moments. Such six-fold degeneracy is split into a Γ_8 quartet and a Γ_7 doublet due to the crystal field effect[54]. The analysis of temperature dependent inelastic neutron scattering and entropy data also revealed that the Γ_8 quartet is the true ground state for the local levels[55], which can be represented in the pseudo-spin $\vec{\sigma}$ and pseudo-orbital $\vec{\tau}$ notation as:

$$\begin{aligned}
 |\tau_z = 1; \sigma_z = 1\rangle &= \sqrt{\frac{5}{6}}|J_z = \frac{5}{2}\rangle + \sqrt{\frac{1}{6}}|J_z = -\frac{3}{2}\rangle, \\
 |\tau_z = 1; \sigma_z = -1\rangle &= \sqrt{\frac{1}{6}}|J_z = \frac{5}{2}\rangle + \sqrt{\frac{5}{6}}|J_z = -\frac{3}{2}\rangle, \\
 |\tau_z = -1; \sigma_z = 1\rangle &= |J_z = \frac{1}{2}\rangle, \\
 |\tau_z = -1; \sigma_z = -1\rangle &= |J_z = -\frac{1}{2}\rangle.
 \end{aligned} \tag{S1}$$

The Γ_8 systems comprise dipoles, quadrupoles, and octupoles, all of which are irreducible representations of the O_h group of the cubic lattice. Both dipolar (magnetic) and quadrupolar order (and likely even octupolar order) may arise via the RKKY interaction between the local multipolar moments[54].

Applying a magnetic field leads to a sequence of two QCPs, which are associated with the magnetic and quadrupolar degrees of freedom respectively [52]. Across each QCP, a jump of the Hall coefficient is found based on extrapolation of its isothermal dependence to the zero-temperature limit[52]. Each jump implicates a destruction of Kondo effect and the concomitant electronic localization-delocalization phase transition at zero temperature.

B. Multipolar Kondo lattice model

We consider a multipolar Kondo lattice model that contains a lattice of local levels with a four-fold degeneracy which can be expressed in term of spin $\vec{\sigma}$ and orbital $\vec{\tau}$ operators:

$$H_{KL} = H_c + H_{f,I} + H_K . \quad (\text{S2})$$

The first part $H_c = \sum_{\vec{k}\sigma\tau} \epsilon_{\vec{k}\sigma\tau} c_{\vec{k}\sigma\tau}^\dagger c_{\vec{k}\sigma\tau}$ defines the kinetic energy of the conduction electrons, and the second part $H_{f,I}$ describes the RKKY interaction among the Γ_8 local levels. For the purpose of convenience and demonstration, we choose $H_{f,I}$ as the Ising type:

$$H_{f,I} = \sum_{ij} [I_{ij}^\sigma \sigma_i^z \sigma_j^z + I_{ij}^\tau \tau_i^z \tau_j^z + I_{ij}^m (\sigma_i^z \otimes \tau_i^z) (\sigma_j^z \otimes \tau_j^z)] , \quad (\text{S3})$$

where, $\vec{\sigma}$, $\vec{\tau}$, and $\vec{\sigma} \otimes \vec{\tau}$ express the spin and orbital operators and their tensor product, respectively, and $I_{ij}^\sigma, I_{ij}^\tau, I_{ij}^m$ are the corresponding coupling constant. Note that here the English letter i, j are indices for sites. The Hamiltonian is essentially the Ising anisotropic version of the Kugel-Khomskii model.

The final part H_K is the Kondo coupling between the local levels and their conduction-electron counterparts:

$$H_K = \sum_i [J_\sigma \vec{\sigma}_i \cdot \vec{\sigma}_{i,c} + J_\tau \vec{\tau}_i \cdot \vec{\tau}_{i,c} + 4J_M (\vec{\sigma}_i \otimes \vec{\tau}_i) \cdot (\vec{\sigma}_{i,c} \otimes \vec{\tau}_{i,c})] , \quad (\text{S4})$$

where the antiferromagnetic Kondo coupling $J_\kappa > 0$ with $\kappa = \sigma, \tau, M$, respectively, describe the interaction of the local levels $\vec{\sigma}$, $\vec{\tau}$, and $\vec{\sigma} \otimes \vec{\tau}$ with the conduction-electron counterparts.

The multipolar Bose-Fermi Kondo model H_{BFK} (Eq. 1) is mapped from the multipolar Kondo lattice model H_{KL} (Eq. S2) under the extended dynamical mean field theory [56–59]. In this procedure, all the sites except for a local impurity are traced out, and the effect of the RKKY interactions between the local multipolar moments is to act effectively as a self-consistent bosonic bath that, along with the self-consistent fermionic bath, are coupled to the local impurity. Specifically, in the EDMFT procedure, the multipolar Kondo lattice is mapped to an effective action that contains the local Kondo couplings as well as the following retarded interactions (where $\beta = 1/k_B T$):

$$\Delta S_{\text{loc},\sigma^z} = -\frac{1}{2} \int_0^\beta d\tau \int_0^\beta d\tau' \sigma^z(\tau) \cdot \chi_{0,\sigma^z}^{-1}(\tau - \tau') \sigma^z(\tau') , \quad (\text{S5})$$

with a self-consistency equation stating that the auto-correlation function of σ^z in the effective action is the same as its local correlation function of the Kondo lattice, and the corresponding

parts for the entwined degrees of freedom τ^z and $(\sigma_i^z \otimes \tau_i^z)$. This action can, via a Caldeira-Leggett procedure [66], be equivalently expressed in a Hamiltonian form, leading to Eq. 5 of the main text. As we described in the main text, prior studies of spin-only Kondo lattice models within the extended dynamical mean field theory have shown that the Kondo destruction fixed points of the Bose-Fermi model without self-consistency but with subohmic ($\epsilon > 0$, *c.f.* Eq. 3 of the main text) are realized in the corresponding Kondo lattice model through the extended dynamical mean field analysis [3, 56]. That the bosonic spectrum is subohmic captures the qualitative physics that the collective fluctuations of the Kondo lattice makes the density of states associated with the bosonic spectrum to be enhanced compared with the ohmic bath induced by the free electron-hole excitations [3, 56].

C. Derivation of the Coulomb gas action and RG equations

We now describe the Coulomb gas action and the procedure of the RG analysis. The Coulomb-gas action is canonical as established for the Kosterlitz-Thouless transition for the case of a single fugacity, and is valid when the fugacity is small (though it is non-perturbative in stiffness constant). Our case is more complex because it involves several fugacities that are coupled together. Nonetheless, the Coulomb-gas action can still be constructed, as graphically illustrated below (Fig. S1), which allows for the systematic construction of the RG equations.

As we mentioned in the main text, because of the Ising-type couplings

$$H_{BK} = g_{\sigma z} \sigma_z \phi_{\sigma z} + g_{\tau z} \tau_z \phi_{\tau z} , \quad (\text{S6})$$

the whole Bose-Fermi Kondo model (Eq. 1) breaks not only the SU(4) symmetry but also the SU(2)×SU(2) symmetry. Therefore, to perform the RG calculation, one need to reduce the symmetry in the Kondo part H_K and introduce much more Kondo couplings. To our purpose, the model with the minimal number of parameters that we need to consider is:

$$H_{BFK} = H_0 + H_{K,o} + H_{BK} , \quad (\text{S7})$$

where H_0 is the non-interacting part for the conduction electron $c_{p,i\alpha}$ and the bosonic bath $\vec{\phi}_{\kappa,q}(\kappa =$

σ, τ, m), and the Kondo coupling $H_{K,o}$ is

$$\begin{aligned}
H_{K,o} = & J_{\sigma z} \sigma_c^z \sigma_c^z + J_{\sigma \perp} (\sigma_c^x \sigma_c^x + \sigma_c^y \sigma_c^y) + J_{\tau z} \tau_c^z \tau_c^z + J_{\tau \perp} (\tau_c^x \tau_c^x + \tau_c^y \tau_c^y) \\
& + 4J_{M1} [(\sigma_x \otimes \tau_x) (\sigma_x \otimes \tau_x)_c + (\sigma_x \otimes \tau_y) (\sigma_x \otimes \tau_y)_c + (\sigma_y \otimes \tau_x) (\sigma_y \otimes \tau_x)_c + (\sigma_y \otimes \tau_y) (\sigma_y \otimes \tau_y)_c] \\
& + 4J_{M2} [(\sigma_z \otimes \tau_x) (\sigma_z \otimes \tau_x)_c + (\sigma_z \otimes \tau_y) (\sigma_z \otimes \tau_y)_c] + 4J_{M3} [(\sigma_x \otimes \tau_z) (\sigma_x \otimes \tau_z)_c + (\sigma_y \otimes \tau_z) (\sigma_y \otimes \tau_z)_c] \\
& + 4J_{M4} [(\sigma_z \otimes \tau_z) (\sigma_z \otimes \tau_z)_c]
\end{aligned} \tag{S8}$$

with $J_{\sigma \perp} = J_{M3}$ and $J_{\tau \perp} = J_{M2}$. Note that compared with the coupling with bosonic bath (Eq. 5), we had already set $g_m = 0$ in the coupling (Eq. S6). In the SI (Sec. E), we will also show that a non-vanishing but small g_m does not modify the structure of our phased diagram based on the RG analysis.

Note that, without the bosonic coupling (Eq. 5), both the Hamiltonian (Eq. 1) and (Eq. S7) admit only a SU(4) Kondo-screened fixed point. In addition, as we will see, tuning the bosonic coupling (Eq. S6) breaks the SU(4) Kondo-screened fixed point directly down to either a spin or orbital SU(2) Kondo-screened fixed point. Therefore, one should expect that how the bare Kondo couplings deviate from the SU(4) symmetric case does not really matter, and the RG analysis of the model (Eq. S7) captures the generic phase diagram of model (Eq. 1).

For the Ising-type bosonic coupling, to perform a controllable RG calculation, one need to map the Bose-Fermi Kondo model into a Coulomb gas type model[60, 61]. The first step to decompose the above Hamiltonian H_{BFK} into the part H_0 that is diagonal in the space of the single impurity states $|\sigma\rangle \otimes |\tau\rangle$, and the other part H_f that is not:

$$H_{BFK} = H_D + H_f, \tag{S9}$$

where H_D is diagonal in the space of the single impurity states $|\sigma\rangle \otimes |\tau\rangle$. We use the notation $|m\rangle = |i\alpha\rangle$ to denote a single impurity state with the orbital $i = 1, 2$ and the spin $\alpha = \uparrow, \downarrow$. Therefore,

$$H_D = \sum_m H_m |m\rangle \langle m|. \tag{S10}$$

Then we rewrite H_m in term of the projection operators $X_{mm} = |m\rangle \langle m| = |i\alpha\rangle \langle i\alpha|$, so that:

$$\begin{aligned}
H_m = & E_m + \sum_n V_m^n c_n^\dagger c_n + \sum_{k,n} E_k c_{k,n}^\dagger c_{k,n} + \sum_q W_q \left(\vec{\phi}_{\sigma,q}^\dagger \cdot \vec{\phi}_{\sigma,q} + \vec{\phi}_{\tau,q}^\dagger \cdot \vec{\phi}_{\tau,q} \right) \\
& + \sum_q F_\sigma^m \left(\phi_{\sigma z,q} + \phi_{\sigma z,-q}^\dagger \right) + \sum_q F_\tau^m \left(\phi_{\tau z,q} + \phi_{\tau z,-q}^\dagger \right),
\end{aligned} \tag{S11}$$

where

$$\begin{aligned}
V_{i\alpha}^{i\alpha} &= \frac{1}{4} (J_{\sigma z} + J_{\tau z} + J_{M4}) , \\
V_{i\alpha}^{i\bar{\alpha}} &= \frac{1}{4} (J_{\tau z} - J_{\sigma z} - J_{M4}) , \\
V_{i\alpha}^{\bar{i}\alpha} &= \frac{1}{4} (J_{\sigma z} - J_{\tau z} - J_{M4}) , \\
V_{i\alpha}^{\bar{i}\bar{\alpha}} &= -\frac{1}{4} (J_{\sigma z} + J_{\tau z} - J_{M4}) ,
\end{aligned} \tag{S12}$$

and

$$\begin{aligned}
F_{\sigma}^{i\uparrow} &= g_{\sigma z} , \\
F_{\sigma}^{i\downarrow} &= -g_{\sigma z} , \\
F_{\tau}^{1\alpha} &= g_{\tau z} , \\
F_{\tau}^{2\alpha} &= -g_{\tau z} .
\end{aligned} \tag{S13}$$

Here we use the over-line symbol to denote the complement of the spin or orbital index.

On the other hand, the flipping part is defined as:

$$H_f = \sum_{m \neq n} Q(m, n), \tag{S14}$$

where

$$Q(m, m) = |m\rangle \langle m| H_f |n\rangle \langle n| \tag{S15}$$

describing the process of flipping from the single impurity state $|n\rangle$ to $|m\rangle$. Specifically,

$$\begin{aligned}
Q(i\alpha, \bar{i}\bar{\alpha}) &= J_{M1} c_{i\alpha}^{\dagger} c_{\bar{i}\bar{\alpha}} |i\alpha\rangle \langle \bar{i}\bar{\alpha}| , \\
Q(i\alpha, i\bar{\alpha}) &= \frac{1}{2} (J_{\sigma\perp} - J_{M3}) c_{i\alpha}^{\dagger} c_{i\bar{\alpha}} |i\alpha\rangle \langle i\bar{\alpha}| + \frac{1}{2} (J_{\sigma\perp} + J_{M3}) c_{i\bar{\alpha}}^{\dagger} c_{i\alpha} |i\alpha\rangle \langle i\bar{\alpha}| = J_{\sigma\perp} c_{i\bar{\alpha}}^{\dagger} c_{i\alpha} |i\alpha\rangle \langle i\bar{\alpha}| , \\
Q(i\alpha, \bar{i}\alpha) &= \frac{1}{2} (J_{\tau\perp} - J_{M2}) c_{i\alpha}^{\dagger} c_{\bar{i}\alpha} |i\alpha\rangle \langle \bar{i}\alpha| + \frac{1}{2} (J_{\tau\perp} + J_{M2}) c_{\bar{i}\alpha}^{\dagger} c_{i\alpha} |i\alpha\rangle \langle \bar{i}\alpha| = J_{\tau\perp} c_{\bar{i}\alpha}^{\dagger} c_{i\alpha} |i\alpha\rangle \langle \bar{i}\alpha|
\end{aligned} \tag{S16}$$

since $J_{\sigma\perp} = J_{M3}$ and $J_{\tau\perp} = J_{M2}$.

Since H_D is diagonal in the single impurity states, after tracing out these local states, the partition function can be expanded in H_f , and the results is:

$$Z = \sum_{n=0}^{\infty} \int_0^{\beta} d\tau_n \dots \int_0^{\tau_{i+1}} d\tau_i \dots \int_0^{\tau_2} d\tau_1 \sum_m A(m; \tau_n, \dots, \tau_1) . \tag{S17}$$

Here the transition amplitude is defined as:

$$\begin{aligned}
A(m; \tau_n, \dots, \tau_1) &= (-1)^n \sum_{m_2, \dots, m_n} \int Dc D\phi \exp[-H_m(\beta - \tau_n)] Q'(m, m_n) \times \dots \\
&\times \exp[-H_{m_{i+1}}(\tau_{i+1} - \tau_i)] Q'(m_{i+1}, m_i) \exp[-H_{m_i}(\tau_i - \tau_{i-1})] \times \dots \\
&\times \exp[-H_{m_2}(\tau_2 - \tau_1)] Q'(m_2, m) \exp[-H_m \tau_1] ,
\end{aligned} \tag{S18}$$

where

$$Q'(m_{i+1}, m_i) = \langle m_{i+1} | H_f | m_i \rangle, \tag{S19}$$

which can be separated as:

$$\langle m | H_f | n \rangle = y'_{m,n} O'(m, n) \tag{S20}$$

with

$$\begin{aligned}
y'_{i\alpha, i\bar{\alpha}} &= J_{M1} , \\
y'_{i\alpha, i\bar{\alpha}} &= \frac{1}{2} (J_{\sigma\perp} + J_{M3}) = J_{\sigma\perp} , \\
y'_{i\alpha, i\bar{\alpha}} &= \frac{1}{2} (J_{\tau\perp} + J_{M2}) = J_{\tau\perp} , \\
O'_{i\alpha, i\bar{\alpha}} &= c_{i\bar{\alpha}}^\dagger c_{i\alpha} , \\
O'_{i\alpha, i\bar{\alpha}} &= c_{i\bar{\alpha}}^\dagger c_{i\alpha} , \\
O'_{i\alpha, i\bar{\alpha}} &= c_{i\bar{\alpha}}^\dagger c_{i\alpha} .
\end{aligned} \tag{S21}$$

Now we can trace out the conduction electron by using the bosonization technique. For our single impurity problem, we only need to consider the s-wave component:

$$c_{i\alpha}(x) = \frac{1}{\sqrt{2\pi a}} e^{-i\theta_{i\alpha}(x)}. \tag{S22}$$

The projected Hamiltonian thus transforms into:

$$H_m = H_c + H_{\phi_\sigma} + H_{\phi_\tau} + E'_m + \sum_n \frac{\delta_m^n}{\pi \rho_0} \left(\frac{d\theta_n(x)}{dx} \right) + \sum_q F_\sigma^m \left(\phi_{\sigma z} + \phi_{\sigma z, -q}^\dagger \right) + \sum_q F_\tau^m \left(\phi_{\tau z, q} + \phi_{\tau z, -q}^\dagger \right) , \tag{S23}$$

where $E'_m = E_m + \Delta E_m$, ρ_0 is the bare conduction electron density of state, and $\delta_{i\alpha}^{j\beta}$ is the phase

shift from the scattering potential:

$$\begin{aligned}
\delta_{i\alpha}^{i\alpha} &= \tan^{-1} (\pi\rho_0 V_{i\alpha}^{i\alpha}) = \tan^{-1} \left[\frac{\pi\rho_0}{4} (J_{\sigma z} + J_{\tau z} + J_{M4}) \right], \\
\delta_{i\alpha}^{i\bar{\alpha}} &= \tan^{-1} (\pi\rho_0 V_{i\alpha}^{i\bar{\alpha}}) = \tan^{-1} \left[\frac{\pi\rho_0}{4} (J_{\tau z} - J_{\sigma z} - J_{M4}) \right], \\
\delta_{i\alpha}^{\bar{i}\alpha} &= \tan^{-1} (\pi\rho_0 V_{i\alpha}^{\bar{i}\alpha}) = \tan^{-1} \left[\frac{\pi\rho_0}{4} (J_{\sigma z} - J_{\tau z} - J_{M4}) \right], \\
\delta_{i\alpha}^{\bar{i}\bar{\alpha}} &= \tan^{-1} (\pi\rho_0 V_{i\alpha}^{\bar{i}\bar{\alpha}}) = \tan^{-1} \left[-\frac{\pi\rho_0}{4} (J_{\sigma z} + J_{\tau z} - J_{M4}) \right].
\end{aligned} \tag{S24}$$

The history dependent potential is treated then through introducing a canonical transformation at each imaginary time:

$$U_\delta = \exp \left(i \frac{\delta}{\pi} \theta \right). \tag{S25}$$

The potential after the canonical transformation is time-independent because of the property:

$$U_\delta^\dagger H_c U_\delta = H_c + \frac{\delta}{\pi\rho_0} \frac{d\theta}{dx}. \tag{S26}$$

We also introduce a similar canonical transformation to the bosonic degree of freedom,

$$\begin{aligned}
U_{W_{\sigma,m}} &= \exp \left(\sum_q \frac{F_\sigma^m}{W_q} \left(\phi_{\sigma z,q} - \phi_{\sigma z,-q}^\dagger \right) \right), \\
U_{W_{\tau,m}} &= \exp \left(\sum_q \frac{F_\tau^m}{W_q} \left(\phi_{\tau z,q} - \phi_{\tau z,-q}^\dagger \right) \right)
\end{aligned} \tag{S27}$$

with the property:

$$\begin{aligned}
U_{W_{\sigma,m}}^\dagger H_{\phi_\sigma} U_{W_{\sigma,m}} &= H_{\phi_\sigma} + \sum_q F_\sigma^m \left(\phi_{\sigma z,q} + \phi_{\sigma z,-q}^\dagger \right), \\
U_{W_{\tau,m}}^\dagger H_{\phi_\tau} U_{W_{\tau,m}} &= H_{\phi_\tau} + \sum_q F_\tau^m \left(\phi_{\tau z,q} + \phi_{\tau z,-q}^\dagger \right).
\end{aligned} \tag{S28}$$

The transition amplitude now reduce to:

$$\begin{aligned}
A(m; \tau_n, \dots, \tau_1) &= Z_c \sum_{m_{n+1}=\alpha_1=m, m_2, \dots, m_{n-1}} y'_{m_{n+1}, \alpha_n} \dots y'_{m_{i+1}, m_i} \dots y'_{m_2, m_1} \\
&\times \exp \left[-E'_m (\tau_1 - \tau_n) - \sum_{i=2}^{n-1} E'_{m_{i+1}} (\tau_{i+1} - \tau_i) \right] \\
&\times \langle O(m_{n+1}, m_n) (\tau_n) \dots O(m_{i+1}, m_i) (\tau_i) \dots O(m_2, m_1) (\tau_1) \rangle \\
&\times \langle B_\sigma(m_{n+1}, m_n) (\tau_n) \dots B_\tau(m_{i+1}, m_i) (\tau_i) \dots B_\sigma(m_2, m_1) (\tau_1) \rangle \\
&\times \langle B_\tau(m_{n+1}, m_n) (\tau_n) \dots B_\tau(m_{i+1}, m_i) (\tau_i) \dots B_\tau(m_2, m_1) (\tau_1) \rangle.
\end{aligned} \tag{S29}$$

Here, for the bosonic part

$$\begin{aligned} B_\sigma(m_{i+1}, M_i)(\tau_i) &= U_{W_\sigma, m_{i+1}} U_{W_\sigma, m_i}^\dagger(\tau_i), \\ B_\tau(m_{i+1}, m_i)(\tau_i) &= U_{W_\tau, m_{i+1}} U_{W_\tau, m_i}^\dagger(\tau_i), \end{aligned} \quad (\text{S30})$$

the correlation function can be reduced into

$$\begin{aligned} \langle B_\sigma(m_{n+1}, m_n)(\tau_n) \dots B_\sigma(m_2, m_1)(\tau_1) \rangle &= U_{W_\sigma, m_{i+1}} U_{W_\sigma, m_i}^\dagger(\tau_i) \\ &= \left\langle \prod_i \exp \left(- \sum_q \frac{F_\sigma^{m_{i+1} m_i}}{W_q} \left(\phi_{\sigma z, q} - \phi_{\sigma z, -q}^\dagger \right) (\tau_i) \right) \right\rangle, \\ &= \left\langle \exp \left(\sum_{ij} C_\sigma(\tau_i - \tau_j) \exp(\Delta_E) \right) \right\rangle \end{aligned} \quad (\text{S31})$$

and similarly

$$\begin{aligned} \langle B_\tau(m_{n+1}, m_n)(\tau_n) \dots B_\tau(m_2, m_1)(\tau_1) \rangle &= U_{W_\tau, m_{i+1}} U_{W_\tau, m_i}^\dagger(\tau_i) \\ &= \left\langle \prod_i \exp \left(- \sum_q \frac{F_\tau^{m_{i+1} m_i}}{W_q} \left(\phi_{\tau z, q} - \phi_{\tau z, -q}^\dagger \right) (\tau_i) \right) \right\rangle \\ &= \left\langle \exp \left(\sum_{ij} C_\tau(\tau_i - \tau_j) \exp(\Delta_E) \right) \right\rangle, \end{aligned} \quad (\text{S32})$$

where

$$\begin{aligned} F_\sigma^{m_{i+1} m_i} &= F_\sigma^{m_{i+1}} - F_\sigma^{m_i}, \\ C_\sigma(\tau_i - \tau_j) &= \sum_q \frac{F_\sigma^{m_{i+1} m_i} F_\sigma^{m_{j+1} m_j}}{W_q^2} \exp(-W_q(\tau_j - \tau_i)) \end{aligned} \quad (\text{S33})$$

and

$$\begin{aligned} F_\tau^{m_{i+1} m_i} &= F_\tau^{m_{i+1}} - F_\tau^{m_i}, \\ C_\tau(\tau_i - \tau_j) &= \sum_q \frac{F_\tau^{m_{i+1} m_i} F_\tau^{m_{j+1} m_j}}{W_q^2} \exp(-W_q(\tau_j - \tau_i)) \end{aligned} \quad (\text{S34})$$

with

$$\sum_q \exp(-W_q \tau) = \frac{K_0}{\tau^{2-\epsilon}}. \quad (\text{S35})$$

On the other hand, for the conduction electron part

$$O(m_{i+1}, m_i)(\tau_i) = \exp(H_c \tau_i) O(m_{i+1}, m_i) \exp(-H_c \tau_i). \quad (\text{S36})$$

Here,

$$O(m_{i+1}, m_i) = \left(\prod_n U_{\delta_{m_{i+1}}^n} \right) O'(m, m_i) \left(\prod_n U_{\delta_{m_i}^n}^\dagger \right), \quad (\text{S37})$$

and for different channels, they are:

$$\begin{aligned}
O(i\alpha, \bar{i}\bar{\alpha}) &= \prod_{j\beta} U_{i\alpha}^{j\beta} c_{\bar{i}\bar{\alpha}}^\dagger c_{i\alpha} \prod_{j\beta} U_{\bar{i}\bar{\alpha}}^{\dagger j\beta} \\
&= \exp \left[\left(\frac{\delta_{i\alpha}^{i\alpha}}{\pi} - \frac{\delta_{\bar{i}\bar{\alpha}}^{i\alpha}}{\pi} - 1 \right) \theta_{i\alpha} + \left(\frac{\delta_{i\alpha}^{i\bar{\alpha}}}{\pi} - \frac{\delta_{\bar{i}\bar{\alpha}}^{i\bar{\alpha}}}{\pi} \right) \theta_{i\bar{\alpha}} + \left(\frac{\delta_{i\alpha}^{\bar{i}\alpha}}{\pi} - \frac{\delta_{\bar{i}\bar{\alpha}}^{\bar{i}\alpha}}{\pi} \right) \theta_{\bar{i}\alpha} + \left(\frac{\delta_{i\alpha}^{\bar{i}\bar{\alpha}}}{\pi} - \frac{\delta_{\bar{i}\bar{\alpha}}^{\bar{i}\bar{\alpha}}}{\pi} + 1 \right) \theta_{\bar{i}\bar{\alpha}} \right], \\
O(i\alpha, i\bar{\alpha}) &= \prod_{j\beta} U_{i\alpha}^{j\beta} c_{i\bar{\alpha}}^\dagger c_{i\alpha} \prod_{j\beta} U_{i\bar{\alpha}}^{\dagger j\beta} \\
&= \exp \left[\left(\frac{\delta_{i\alpha}^{i\alpha}}{\pi} - \frac{\delta_{i\bar{\alpha}}^{i\alpha}}{\pi} - 1 \right) \theta_{i\alpha} + \left(\frac{\delta_{i\alpha}^{i\bar{\alpha}}}{\pi} - \frac{\delta_{i\bar{\alpha}}^{i\bar{\alpha}}}{\pi} + 1 \right) \theta_{i\bar{\alpha}} + \left(\frac{\delta_{i\alpha}^{\bar{i}\alpha}}{\pi} - \frac{\delta_{i\bar{\alpha}}^{\bar{i}\alpha}}{\pi} \right) \theta_{\bar{i}\alpha} + \left(\frac{\delta_{i\alpha}^{\bar{i}\bar{\alpha}}}{\pi} - \frac{\delta_{i\bar{\alpha}}^{\bar{i}\bar{\alpha}}}{\pi} \right) \theta_{\bar{i}\bar{\alpha}} \right], \\
O(i\alpha, \bar{i}\alpha) &= \prod_{j\beta} U_{i\alpha}^{j\beta} c_{\bar{i}\alpha}^\dagger c_{i\alpha} \prod_{j\beta} U_{\bar{i}\alpha}^{\dagger j\beta} \\
&= \exp \left[\left(\frac{\delta_{i\alpha}^{i\alpha}}{\pi} - \frac{\delta_{\bar{i}\alpha}^{i\alpha}}{\pi} - 1 \right) \theta_{i\alpha} + \left(\frac{\delta_{i\alpha}^{i\bar{\alpha}}}{\pi} - \frac{\delta_{\bar{i}\alpha}^{i\bar{\alpha}}}{\pi} \right) \theta_{i\bar{\alpha}} + \left(\frac{\delta_{i\alpha}^{\bar{i}\alpha}}{\pi} - \frac{\delta_{\bar{i}\alpha}^{\bar{i}\alpha}}{\pi} + 1 \right) \theta_{\bar{i}\alpha} + \left(\frac{\delta_{i\alpha}^{\bar{i}\bar{\alpha}}}{\pi} - \frac{\delta_{\bar{i}\alpha}^{\bar{i}\bar{\alpha}}}{\pi} \right) \theta_{\bar{i}\bar{\alpha}} \right].
\end{aligned} \tag{S38}$$

We can rewrite these term as:

$$O(m, n) = \exp \left[i \sum_r e_{mn}^r \theta_r \right]. \tag{S39}$$

After all of these, the partition function is mapped into:

$$\frac{Z}{Z_0} = \sum_{n=0}^{\infty} \sum_{m_{n+1}=m_1=m, m_2, \dots, m_{n-1}} \int_{\xi_0}^{\beta-\xi_0} \frac{d\tau_n}{\xi_0} \dots \int_{\xi_0}^{\tau_{i+1}-\xi_0} \frac{d\tau_i}{\xi_0} \dots \int_{\xi_0}^{\tau_2-\xi_0} \frac{d\tau_1}{\xi_0} \exp[-S(\tau_1, \dots, \tau_n)] \tag{S40}$$

with a Coulomb gas type action:

$$\begin{aligned}
S(\tau_1, \dots, \tau_n) &= - \sum_i \ln y_{m_i, m_{i+1}} + \sum_i h_{m_{i+1}} \frac{\tau_{i+1} - \tau_i}{\xi_0} \\
&+ \sum_{i < j} [K_{m_i, m_j} + K_{m_{i+1}, m_{j+1}} - K_{m_i, m_{j+1}} - K_{m_{i+1}, m_j}] \ln \frac{\tau_j - \tau_i}{\xi_0} \\
&- \sum_{i < j} [M_{m_i, m_j}^\sigma + M_{m_{i+1}, m_{j+1}}^\sigma - M_{m_i, m_{j+1}}^\sigma - M_{m_{i+1}, m_j}^\sigma] \left[\left(\frac{\tau_j - \tau_i}{\xi_0} \right)^\epsilon - 1 \right] \\
&- \sum_{i < j} [M_{m_i, m_j}^\tau + M_{m_{i+1}, m_{j+1}}^\tau - M_{m_i, m_{j+1}}^\tau - M_{m_{i+1}, m_j}^\tau] \left[\left(\frac{\tau_j - \tau_i}{\xi_0} \right)^\epsilon - 1 \right],
\end{aligned} \tag{S41}$$

where $h_m \propto E'_m$, ξ_0 is the ultraviolet cutoff, and

$$\begin{aligned}
y_{m,n} &= y'_{m,n} \xi_0, \\
K_{m,n} &= -\frac{1}{2} \sum_r (e_{mn}^r)^2, \\
M_{m,n}^\sigma &= -\frac{1}{2} \sum_q (F_\sigma^{mn})^2, \\
M_{m,n}^\tau &= -\frac{1}{2} \sum_q (F_\tau^{mn})^2.
\end{aligned} \tag{S42}$$

By following these definitions, for the Bose-Fermi Kondo model (Eq. S7) the non-vanishing fugacity $y_{m,n}$ and stiffness $K_{m,n}$, $M_{m,n}^\sigma$ and $M_{m,n}^\tau$ are:

$$\begin{aligned}
y_{i\alpha, \bar{i}\bar{\alpha}} &\equiv y_1 = \xi_0 J_{M1}, \\
y_{i\alpha, i\bar{\alpha}} &\equiv y_2 = \xi_0 J_{\sigma\perp}, \\
y_{i\alpha, \bar{i}\alpha} &\equiv y_3 = \xi_0 J_{\tau\perp}, \\
K_{i\alpha, \bar{i}\bar{\alpha}} &\equiv -K_1 = -f_1(J_{\sigma z}, J_{\tau z}, J_{M4}), \\
K_{i\alpha, i\bar{\alpha}} &\equiv -K_2 = -f_2(J_{\sigma z}, J_{\tau z}, J_{M4}), \\
K_{i\alpha, \bar{i}\alpha} &\equiv -K_3 = -f_3(J_{\sigma z}, J_{\tau z}, J_{M4}), \\
M_{i\alpha, \bar{i}\bar{\alpha}}^\sigma &= M_{i\alpha, i\bar{\alpha}}^\sigma \equiv -M^\sigma = -\Gamma(\epsilon) g_{\sigma z}^2, \\
M_{i\alpha, \bar{i}\bar{\alpha}}^\tau &= M_{i\alpha, \bar{i}\alpha}^\tau \equiv -M^\tau = -\Gamma(\epsilon) g_{\tau z}^2,
\end{aligned} \tag{S43}$$

where $\Gamma(\epsilon)$ is a ϵ dependent $O(1)$ constant. The explicit expression of $K_{1,2,3}$ is complicated but unnecessary, and can be derived from Eq. S38, where the phase shifts are known in Eq. S24. The only few things that matter are that they depend only on indices-preserving coupling $J_{\sigma z, \tau z, M4}$, and the range of their bare value is $f_{1,2,3}(J_{\sigma z}, J_{\tau z}, J_{M4}) \in (0, 3)$.

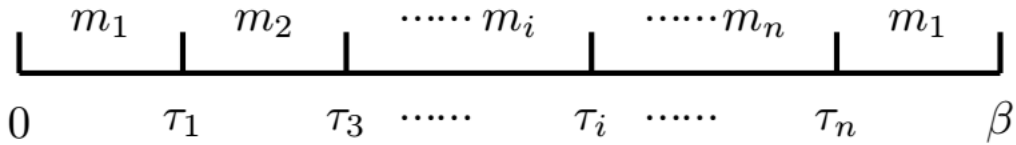


FIG. S1. Hopping sequences of the local states along the imaginary time axis. Here τ_i , for $i = 1, \dots, n$, labels the imaginary time at which the local state hops from $|m_i\rangle$ to $|m_{i+1}\rangle$.

The Coulomb gas action (Eq. S41) is a summation over all possible histories of the local degrees of freedom which fluctuate between $n + 1$ local states $|m\rangle$. Each history, labeled by

$\{m_1, \dots, m_n; \tau_1, \dots, \tau_n\}$, is a sequence of the transition between the local states from m_1 through m_n taking place at the time $\tau_1 < \dots < \tau_n$, as illustrated in Fig. S1. (The periodic boundary condition has been imposed.) The action (Eq. S41) gives the statistical weight of such a history. We can interpret Eq. S41 in terms of a partition function of a plasma of kinks with interactions. It has multiple components of “stiffness” $K_{m,n}$ and $M_{m,n}^{\tau/\sigma}$ and “fugacity” $y_{m,n}$, as defined in (Eq. S42). For such a Coulomb gas action (Eq. S41), one can perform the RG calculation by integrating out the degrees of freedom within the cutoff shell $[\xi_0, \xi_0 + \xi_0 dl]$ (Refs. 61, 62, 65, 67, 68). In the absence of the $M_{m,n}^{\tau/\sigma}$ terms, the RG beta functions have been derived in Ref. 67. With the $M_{m,n}^{\tau/\sigma}$ terms, the same technique is still applicable [62, 63], and the final beta functions are:

$$\begin{aligned}
\frac{dy_1}{dl} &= (1 - K_1 - M^\sigma - M^\tau) y_1 + 2y_2 y_3 , \\
\frac{dy_2}{dl} &= (1 - K_2 - M^\sigma) y_2 + 2y_1 y_3 , \\
\frac{dy_3}{dl} &= (1 - K_3 - M^\tau) y_3 + 2y_1 y_2 , \\
\frac{dK_1}{dl} &= -2y_1^2 (2K_1) - 2y_2^2 (K_1 + K_2 - K_3) - 2y_3^2 (K_1 + K_3 - K_2) , \\
\frac{dK_2}{dl} &= -2y_1^2 (K_2 + K_1 - K_3) - 2y_2^2 (2K_2) - 2y_3^2 (K_2 + K_3 - K_1) , \\
\frac{dK_3}{dl} &= -2y_1^2 (K_3 + K_1 - K_2) - 2y_2^2 (K_3 + K_2 - K_1) - 2y_3^2 (2K_3) , \\
\frac{dM^\sigma}{dl} &= (\epsilon - 4y_1^2 - 4y_2^2) M^\sigma , \\
\frac{dM^\tau}{dl} &= (\epsilon - 4y_1^2 - 4y_3^2) M^\tau .
\end{aligned} \tag{S44}$$

D. RG analysis and the generic phase diagram

In this section, we give a detailed RG analysis of the beta functions (Eq. S44). We will identify the fixed points of the beta functions (Eq. S44) by using ϵ as the control parameter. The relative

stability of these fixed points are analysed through the eigenvalues and eigenvectors of the matrix:

$$W = \begin{pmatrix} \frac{\partial \beta_{y_1}}{\partial y_1} & \frac{\partial \beta_{y_1}}{\partial y_2} & \frac{\partial \beta_{y_1}}{\partial y_3} & \frac{\partial \beta_{y_1}}{\partial K_1} & \frac{\partial \beta_{y_1}}{\partial K_2} & \frac{\partial \beta_{y_1}}{\partial K_3} & \frac{\partial \beta_{y_1}}{\partial M^\sigma} & \frac{\partial \beta_{y_1}}{\partial M^\tau} \\ \frac{\partial \beta_{y_2}}{\partial y_1} & \frac{\partial \beta_{y_2}}{\partial y_2} & \frac{\partial \beta_{y_2}}{\partial y_3} & \frac{\partial \beta_{y_2}}{\partial K_1} & \frac{\partial \beta_{y_2}}{\partial K_2} & \frac{\partial \beta_{y_2}}{\partial K_3} & \frac{\partial \beta_{y_2}}{\partial M^\sigma} & \frac{\partial \beta_{y_2}}{\partial M^\tau} \\ \frac{\partial \beta_{y_3}}{\partial y_1} & \frac{\partial \beta_{y_3}}{\partial y_2} & \frac{\partial \beta_{y_3}}{\partial y_3} & \frac{\partial \beta_{y_3}}{\partial K_1} & \frac{\partial \beta_{y_3}}{\partial K_2} & \frac{\partial \beta_{y_3}}{\partial K_3} & \frac{\partial \beta_{y_3}}{\partial M^\sigma} & \frac{\partial \beta_{y_3}}{\partial M^\tau} \\ \frac{\partial \beta_{K_1}}{\partial y_1} & \frac{\partial \beta_{K_1}}{\partial y_2} & \frac{\partial \beta_{K_1}}{\partial y_3} & \frac{\partial \beta_{K_1}}{\partial K_1} & \frac{\partial \beta_{K_1}}{\partial K_2} & \frac{\partial \beta_{K_1}}{\partial K_3} & \frac{\partial \beta_{K_1}}{\partial M^\sigma} & \frac{\partial \beta_{K_1}}{\partial M^\tau} \\ \frac{\partial \beta_{K_2}}{\partial y_1} & \frac{\partial \beta_{K_2}}{\partial y_2} & \frac{\partial \beta_{K_2}}{\partial y_3} & \frac{\partial \beta_{K_2}}{\partial K_1} & \frac{\partial \beta_{K_2}}{\partial K_2} & \frac{\partial \beta_{K_2}}{\partial K_3} & \frac{\partial \beta_{K_2}}{\partial M^\sigma} & \frac{\partial \beta_{K_2}}{\partial M^\tau} \\ \frac{\partial \beta_{K_3}}{\partial y_1} & \frac{\partial \beta_{K_3}}{\partial y_2} & \frac{\partial \beta_{K_3}}{\partial y_3} & \frac{\partial \beta_{K_3}}{\partial K_1} & \frac{\partial \beta_{K_3}}{\partial K_2} & \frac{\partial \beta_{K_3}}{\partial K_3} & \frac{\partial \beta_{K_3}}{\partial M^\sigma} & \frac{\partial \beta_{K_3}}{\partial M^\tau} \\ \frac{\partial \beta_{M^\sigma}}{\partial y_1} & \frac{\partial \beta_{M^\sigma}}{\partial y_2} & \frac{\partial \beta_{M^\sigma}}{\partial y_3} & \frac{\partial \beta_{M^\sigma}}{\partial K_1} & \frac{\partial \beta_{M^\sigma}}{\partial K_2} & \frac{\partial \beta_{M^\sigma}}{\partial K_3} & \frac{\partial \beta_{M^\sigma}}{\partial M^\sigma} & \frac{\partial \beta_{M^\sigma}}{\partial M^\tau} \\ \frac{\partial \beta_{M^\tau}}{\partial y_1} & \frac{\partial \beta_{M^\tau}}{\partial y_2} & \frac{\partial \beta_{M^\tau}}{\partial y_3} & \frac{\partial \beta_{M^\tau}}{\partial K_1} & \frac{\partial \beta_{M^\tau}}{\partial K_2} & \frac{\partial \beta_{M^\tau}}{\partial K_3} & \frac{\partial \beta_{M^\tau}}{\partial M^\sigma} & \frac{\partial \beta_{M^\tau}}{\partial M^\tau} \end{pmatrix}. \quad (\text{S45})$$

We will also illustrate the generic phase diagram Fig. 3(a) based on our RG analysis.

RG analysis. In the ϵ expansion, the ϵ serve as a small control parameter. We will express the fixed point in term of the ϵ up to the leading order $\sqrt{\epsilon}$. By solving the zeros of the beta functions (Eq. S44), the fixed points can be identified:

$$\begin{aligned} \mathbf{R1} : y_1 = 0, y_2 = y_3 = \frac{\sqrt{\epsilon}}{2}, K_1 = K_2 = K_3 = 0, M^\sigma = M^\tau = 1, \\ \mathbf{R2} : y_1 = \frac{\sqrt{\epsilon}}{2}, y_2 = 0, y_3 = 0, K_2 = K_3, K_1 = 0, M^\sigma + M^\tau = 1, \end{aligned} \quad (\text{S46})$$

where the RG trajectory around **R2** can flow toward **R1**. Other fixed points includes

$$\mathbf{E1} : y_1 = 0, y_2 = \frac{\sqrt{\epsilon}}{2}, y_3 = 0, K_1 = K_3, K_2 = 0, M^\sigma = 1, M^\tau = 0, \quad (\text{S47})$$

and

$$\mathbf{E2} : y_1 = 0, y_2 = 0, y_3 = \frac{\sqrt{\epsilon}}{2}, K_1 = K_2, K_3 = 0, M^\sigma = 0, M^\tau = 1, \quad (\text{S48})$$

and both of the fixed points **E1** and **E2** are unstable and the RG trajectory around them can flow toward **R1** and **R2**. Finally, there is a unstable fixed points

$$\mathbf{E3} : y_1 = y_2 = y_3 = 0, M^\sigma = M^\tau = 0. \quad (\text{S49})$$

We will ignore this fixed point in the following, since it is the most unstable fixed points.

Among the fixed points listed in the Eqs. S46-S49, the fixed point **R1** is the most stable one. However, the fixed point **R1** is actually still not a generic critical point, since there are two relevant directions $\vec{v}_{1,2}$ around it. The first one is:

$$\vec{v}_1 = \frac{1}{2\sqrt{2}}\hat{y}_2 - \frac{1}{2\sqrt{2}}\hat{y}_3 + \hat{M}^\sigma - \hat{M}^\tau \quad (\text{S50})$$

which has the associated eigenvalue scaling dimension $\sqrt{2\epsilon}$ and can flow toward either the orbital KS fixed point:

$$\mathbf{K1} : y_2 \rightarrow \infty, y_1 = y_3 = 0, K_1 = K_2 = K_3, M^\sigma = 0, M^\tau \rightarrow \infty$$

or spin KS fixed point:

$$\mathbf{K2} : y_3 \rightarrow \infty, y_1 = y_2 = 0, K_1 = K_2 = K_3 = 0, M^\sigma \rightarrow \infty, M^\tau = 0 .$$

On the other hand, the second relevant direction is (we express each non-vanishing coefficients up to the leading order $\sqrt{\epsilon}$):

$$\vec{v}_2 = \frac{\sqrt{\epsilon}}{2}\hat{y}_1 + \frac{1}{2\sqrt{2}}\hat{y}_2 + \frac{1}{2\sqrt{2}}\hat{y}_3 - \hat{M}^\sigma - \hat{M}^\tau \quad (\text{S51})$$

which has associated scaling dimension $\sqrt{2\epsilon}$ (up to the leading order $\sqrt{\epsilon}$) and flows toward either the strong coupling SU(4) Kondo-screened (KS) fixed point

$$\mathbf{K3} : y_1, y_2, y_3 \rightarrow \infty, K_1 = K_2 = K_3 = 0, M^\sigma = M^\tau = 0$$

or the spin and orbital Kondo-destroyed (KD) phase

$$\mathbf{G} : y_1 = y_2 = y_3 = 0, M^\sigma \rightarrow \infty, M^\tau \rightarrow \infty .$$

The stability of the strong coupling fixed points **K1**, **K2**, **K3**, and **G** can be studied through the stability matrix W (Eq. S45). This analysis shows that the fixed points are stable against other small perturbations and thus characterize the phase of matter. Accordingly, there should be other generic critical points separate these phases. Since there are two relevant directions around **R1**, there should be four generic critical points separating these phase.

Moreover, besides flowing toward to **R1**, **K1**, **K2** and **G**, by exploring the relevant direction around the fixed point **E1** one can also checks that the RG trajectory around it can also flow toward $M^\tau \rightarrow \infty$ ($M^\sigma \rightarrow \infty$), and thus approach to:

$$\mathbf{F1} : y_1 = 0, y_2 = \frac{\sqrt{\epsilon}}{2}, y_3 = 0, K_1 = K_2 = K_3 = 0, M^\sigma = 1, M^\tau \rightarrow \infty .$$

For the **F1**, except the beta function dM^τ/dl , other beta functions remain zero. As a result, **F1** corresponds to a fixed point at the large M^τ regime. By study the nearby RG trajectory through

the matrix W in Eq. S45, one can conclude that fixed point **F1** actually corresponds to a generic critical point separate the spin and orbital KD phase **G** and the orbital KS phase **K1**.

Similarly the RG trajectory around **E2** can flow toward:

$$\mathbf{F2}: y_1 = 0, y_2 = 0, y_3 = \frac{\sqrt{\epsilon}}{2}, K_1 = K_2 = K_3 = 0, M^\tau = 1, M^\sigma \rightarrow \infty,$$

which is a generic critical point between the spin and orbital KD phase **G** and the orbital KS phase **K3**.

The whole RG flow structure is summarized in Fig. 5 of the main text, where the blue boxes are the critical points **F1-F2** corresponding to the phase transitions from spin and orbital KD phase to spin or orbital KS phases. One can see that the spin and orbital KD phase **G** can transit to different kinds of strong Kondo coupling fixed points **K1**, **K2**, and **K3**. Note that because the fixed point **R1**, denoted as the red box in Fig. 5, is not a generic but a multi-critical point, the phase transition between spin and orbital KS phase **K3** and spin and orbital KD phase **G** should be a fine-tuned one. Again, since the Kondo screened fixed points **K1**, **K2**, **K3** are stable fixed points, there should be some generic critical points (denoted as the orange boxes **X1** and **X2** in Fig. 5 separating them, even though their exact directions is unknown in this scheme unlike the generic critical point **F1** and **F2**. Based on the whole RG flow structure Fig. 5, the generic phase diagram is summarized in Fig. 3. Note that in Fig. 5, we neglected the fixed point **R2**, **E1**, **E2**, and **E3** since these fixed points do not influence the RG structure. We present the relative RG flow structure among the fixed points **R1**, **E1**, **F1**, **K1**, and **G** in Fig. S2.

We emphasize that the RG flow structure Fig. 5 is rigorously derived through the matrix W (Eq. S45). However, due to the huge number of the coupling constants, it is not easy to visualize the full RG flow structure. In the following, we are going to elaborate these results in a reduced but more transparent and visible way.

Transition to the SU(4) Kondo-screened phase. To illustrate the transition between the spin and orbital KD phase to the SU(4) KS phase, we choose to scan the RG flow structure by taking $g_{\sigma z} = g_{\tau z} = g$, which corresponds to the trajectory denoted as the arrow (I) in Fig. 3(a).

Since along this direction, the beta functions (Eq. S44) are invariant under $\sigma \leftrightarrow \tau$, one can set

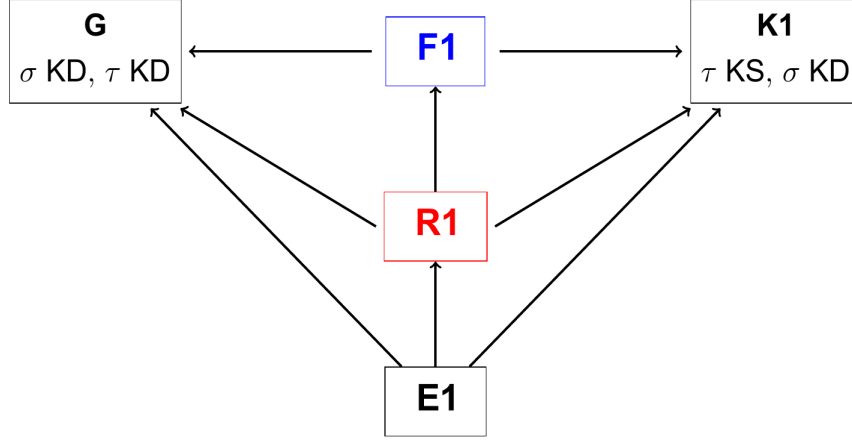


FIG. S2. **The structure of the renormalization-group flow.** The relative RG flow structure among the fixed points **R1**, **E1**, **F1**, **K1**, and **G**.

$y_2 = y_3 = y$ and $K_2 = K_3 = K$. The beta functions (Eq. S44) thus can be reduced to:

$$\begin{aligned}
 \frac{dy_1}{dl} &= (1 - K_1 - 2M) y_1 + 2y^2 , \\
 \frac{dy}{dl} &= (1 - K - M) y + 2y_1 y , \\
 \frac{dK_1}{dl} &= -2y_1^2 (2K_1) - 4y^2 (K_1) , \\
 \frac{dK}{dl} &= -2y_1^2 (K_1) - 4y^2 (2K) + 2y^2 (K_1) , \\
 \frac{dM}{dl} &= (\epsilon - 4y_1^2 - 4y^2) M .
 \end{aligned} \tag{S52}$$

Note that the fugacity y_1 flips both spin and orbital part, while the fugacity y flips only the spin or orbital index. As a result, the beta functions of y_1 and y involve y^2 and $y_1 y$, respectively.

From the beta functions Eq. S52, one can see that the coupling constant K_1 flows to 0 no matter the initial values, and thus the beta functions can be further reduced into:

$$\begin{aligned}
 \frac{dy_1}{dl} &= (1 - 2M) y_1 + 2y^2 , \\
 \frac{dy}{dl} &= (1 - K - M) y + 2y_1 y , \\
 \frac{dK}{dl} &= -4y^2 (2K) , \\
 \frac{dM}{dl} &= (\epsilon - 4y_1^2 - 4y^2) M ,
 \end{aligned} \tag{S53}$$

and again, $K \rightarrow 0$ no matter the initial values, so in the end we derive the reduced beta functions

Eq. 7:

$$\begin{aligned}
\frac{dy_1}{dl} &= (1 - 2M) y_1 + 2y^2 , \\
\frac{dy}{dl} &= (1 - M) y + 2y_1 y , \\
\frac{dM}{dl} &= (\epsilon - 4y_1^2 - 4y^2) M .
\end{aligned} \tag{S54}$$

From these reduced beta functions (Eq. S54), we identify the generic critical point $(y_1^*, y^*, M^*) = \left(\frac{-1 + \sqrt{1 + 12\epsilon}}{12}, \frac{\sqrt{-1 + 12\epsilon + \sqrt{1 + 12\epsilon}}}{6\sqrt{2}}, \frac{5 + \sqrt{1 + 12\epsilon}}{6} \right) \cong \left(0, \frac{\sqrt{\epsilon}}{2}, 1 \right)$ up to the order $\sqrt{\epsilon}$. This critical point corresponds to the critical point **R1** in Fig. 5, and separates the spin and orbital KD phase from the SU(4) KS phase.

Transition to spin or orbital Kondo-screened phase. Here we aim to illustrate the transition between the spin and orbital KD phase and the spin or orbital KS phase. We firstly focus on the RG trajectory around the critical point **R1** where $g_{\sigma z} = g_{\tau z} = g^*$ between the spin and orbital KD **G** and SU(4) KS phases **K3**.

As mentioned, any small asymmetry between $g_{\tau z}$ and $g_{\sigma z}$ around **R1** actually is relevant in RG sense. Suppose we keep every parameters fixed but just slightly increase the coupling constant $g_{\tau z}$, that is, $g_{\tau z} > g_{\sigma z} = g^*$, then the RG trajectory will flow toward to $g_{\tau z} \rightarrow \infty$. We can then vary $g_{\sigma z}$ to explore the RG trajectory. The corresponding trajectories in the phase diagram are denoted as the arrow (II) in Fig. 3(a). Around this trajectory, according to the beta functions (Eq. S44), y_1 and y_3 must both flow to 0 and both are irrelevant since $g_{\tau z} \rightarrow \infty$. The beta functions can thus be reduced into:

$$\begin{aligned}
\frac{dy_2}{dl} &= (1 - K_2 - M^\sigma) y_2 , \\
\frac{dK_1}{dl} &= -2y_2^2 (K_1 + K_2 - K_3) , \\
\frac{dK_2}{dl} &= -2y_2^2 (2K_2) , \\
\frac{dK_3}{dl} &= -2y_2^2 (K_3 + K_2 - K_1) , \\
\frac{dM^\sigma}{dl} &= (\epsilon - 4y_2^2) M^\sigma .
\end{aligned} \tag{S55}$$

by which one can see that $K_2 \rightarrow 0$, and again the beta functions can be further reduced into:

$$\begin{aligned}
\frac{dy_2}{dl} &= (1 - M^\sigma) y_2 , \\
\frac{dK_1}{dl} &= -2y_2^2 (K_1 - K_3) , \\
\frac{dK_3}{dl} &= -2y_2^2 (K_3 - K_1) , \\
\frac{dM^\sigma}{dl} &= (\epsilon - 4y_2^2) M^\sigma .
\end{aligned}
\tag{S56}$$

From the reduced beta functions (Eq. S56), one can immediately conclude that the K_1 and K_3 flow to the fixed point $K_1 = K_3 = k_\tau$, where k_τ is a constant. As a result, the final reduced beta functions are indeed Eq. 8, from which one can find a generic critical point $(y_2^*, M^{\sigma*}) = \left(\frac{\sqrt{\epsilon}}{2}, 1\right)$ with the scaling dimensions $\frac{1}{2}\sqrt{\epsilon}(\sqrt{\epsilon} + \sqrt{8 + \epsilon}) \cong \sqrt{2\epsilon}$ (up to the order $\sqrt{\epsilon}$) that corresponds to the fixed point **F2** in Fig. 5 and separates the spin and orbital KD phase from the spin KS phase. The RG flow diagram of the reduced beta functions (Eq. 8) on the $J_{\sigma\perp} - g_{\sigma z}$ plane is shown in Fig. S3.

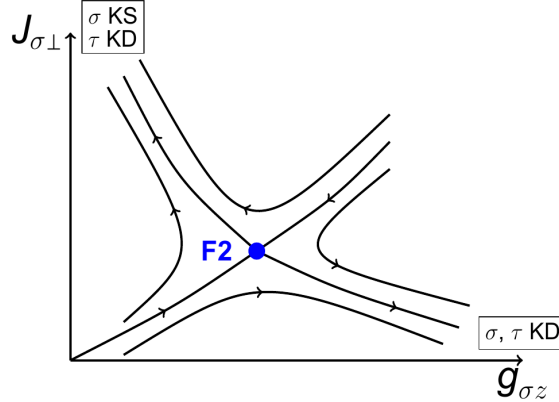


FIG. S3. **A renormalization-group flow.** RG flow diagram of the reduced beta functions (Eq. 8) on the $J_{\sigma\perp} - g_{\sigma z}$ plane.

Transition between spin or orbital KS phase and SU(4) KS phase. Finally, we would like to establish the transition between the spin or orbital KS phase and the SU(4) KS phase, which correspond to the trajectories III in Fig. 3(a). As discussed in the main text, because the strong Kondo coupling fixed points **K1**, **K2**, and **K3** are stable fixed points, there should be other generic critical points, denoted as orange boxes **X1** and **X2**, separating them.

Again, we focus on the RG trajectory around the critical point **R1** where $g_{\sigma z} = g_{\tau z} = g^*$ between the spin and orbital KD **G** and SU(4) KS phases **K3**. If we keep every parameters fixed

but just slightly decrease the coupling constant $g_{\sigma z}$, that is, $g_{\sigma z} < g_{\tau z} = g^*$, then the RG trajectory will flow toward to $g_{\sigma z} \rightarrow 0$. We can then vary $g_{\tau z}$ to explore the RG trajectory. The corresponding trajectories in the phase diagram are denoted as the arrow (III) in Fig. 3(a). As we will see later, the assumption that $g_{\sigma z} \rightarrow 0$ is legitimate since $g_{\sigma z}$ is generally irrelevant around $g_{\sigma z} = 0$.

However, unlike **R1** and **F1**, the real locations of the **X1** is hard to identify directly from the beta functions (Eq. S44). To proceed, we exploit one more property of the critical point **R1**, that is, $y_1 \sim 0$, $y_{2,3} \sim \frac{\sqrt{\epsilon}}{2}$ around **R1**. Near the vicinity of **R1**, one can thus neglect the higher order terms of $\sqrt{\epsilon}$ in the beta functions (Eq. S44). To simplify the analysis, we also set the new variables:

$$\begin{aligned} u_3 &= K_1 + K_2 - K_3, \\ u_2 &= K_1 + K_3 - K_2, \\ u_1 &= K_2 + K_3 - K_1. \end{aligned} \tag{S57}$$

The beta functions (Eq. S44) then become:

$$\begin{aligned} \frac{dy_1}{dl} &= \left(1 - \frac{u_2}{2} - \frac{u_3}{2} - M^\tau\right) y_1, \\ \frac{dy_2}{dl} &= \left(1 - \frac{u_1}{2} - \frac{u_3}{2}\right) y_2, \\ \frac{dy_3}{dl} &= \left(1 - \frac{u_1}{2} - \frac{u_2}{2} - M^\tau\right) y_3, \\ \frac{du_3}{dl} &= -4(y_1^2 + y_2^2) u_3, \\ \frac{du_2}{dl} &= -4(y_1^2 + y_3^2) u_2, \\ \frac{du_1}{dl} &= -4(y_2^2 + y_3^2) u_1, \\ \frac{dM^\sigma}{dl} &= (\epsilon - 4y_1^2 - 4y_2^2) M^\sigma, \\ \frac{dM^\tau}{dl} &= (\epsilon - 4y_1^2 - 4y_3^2) M^\tau. \end{aligned} \tag{S58}$$

by which one can see that u_1 , u_2 , and u_3 are generally irrelevant and flow to zero, and thus the resulting beta functions are

$$\begin{aligned} \frac{dy_1}{dl} &= (1 - M^\tau) y_1, \\ \frac{dy_2}{dl} &= y_2, \\ \frac{dy_3}{dl} &= (1 - M^\tau) y_3, \\ \frac{dM^\sigma}{dl} &= (\epsilon - 4y_1^2 - 4y_2^2) M^\sigma, \\ \frac{dM^\tau}{dl} &= (\epsilon - 4y_1^2 - 4y_3^2) M^\tau. \end{aligned} \tag{S59}$$

From the reduced beta functions (Eq. S59), one can immediately conclude that $y_2 \rightarrow \infty$, and thus M^σ is indeed irrelevant around $M^\sigma \rightarrow 0$. The final reduced beta functions are

$$\begin{aligned}\frac{dy_1}{dl} &= (1 - M^\tau) y_1, \\ \frac{dy_3}{dl} &= (1 - M^\tau) y_3, \\ \frac{dM^\tau}{dl} &= (\epsilon - 4y_1^2 - 4y_3^2) M^\tau.\end{aligned}\tag{S60}$$

from which one can identify a critical line $(y_1^*, y_3^*, M^{\tau*}) = \left(a, \frac{\sqrt{\epsilon - 4a^2}}{2}, 1\right)$ where a is a constant, which has one relevant direction with the associated scaling dimension $\sqrt{2\epsilon}$ and separates the spin and orbital KS phase from the spin KS phase and corresponds to the critical point **X1** in Fig. 5. The RG flow diagram of reduced beta functions (Eq. S60) is plotted in Fig. S4. By a parallel analysis, the transition between the spin and orbital KS phase and the orbital KS phase can also be established.

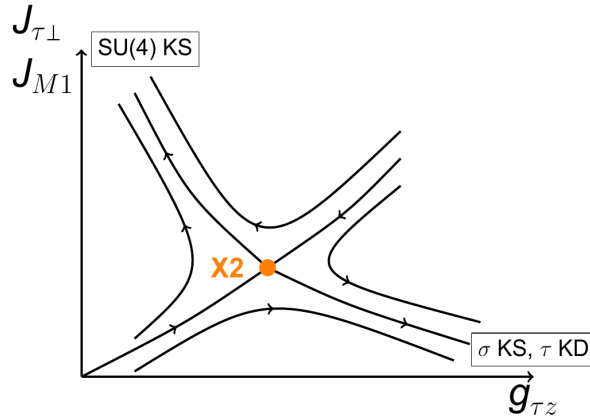


FIG. S4. **A separate renormalization-group flow.** The RG flow diagram of the reduced beta functions (Eq. S60).

E. RG analysis with a small cross-product term g_m

In this section, we aim to study the stability of the phase diagram Fig. 3(a) under a small cross-product term $g_m (\sigma_z \otimes \tau_z) \phi_m$ through RG analysis. In other words, we derive the beta functions of the Bose-Fermi-Kondo model H_{BFK} where the coupling with the bosonic bath is modified as:

$$H_{BK} = g_{\sigma z} \sigma_z \phi_{\sigma z} + g_{\tau z} \tau_z \phi_{\tau z} + g_m (\sigma_z \otimes \tau_z) \phi_m.\tag{S61}$$

After mapping the model into a Coulomb-gas type action, one can derive the beta functions:

$$\begin{aligned}
\frac{dy_1}{dl} &= (1 - K_1 - M^\sigma - M^\tau) y_1 + 2y_2y_3 , \\
\frac{dy_2}{dl} &= (1 - K_2 - M^\sigma - M^m) y_2 + 2y_1y_3 , \\
\frac{dy_3}{dl} &= (1 - K_3 - M^\tau - M^m) y_3 + 2y_1y_2 , \\
\frac{dK_1}{dl} &= -2y_1^2 (2K_1) - 2y_2^2 (K_1 + K_2 - K_3) - 2y_3^2 (K_1 + K_3 - K_2) , \\
\frac{dK_2}{dl} &= -2y_1^2 (K_2 + K_1 - K_3) - 2y_2^2 (2K_2) - 2y_3^2 (K_2 + K_3 - K_1) , \\
\frac{dK_3}{dl} &= -2y_1^2 (K_3 + K_1 - K_2) - 2y_2^2 (K_3 + K_2 - K_1) - 2y_3^2 (2K_3) , \\
\frac{dM^\sigma}{dl} &= (\epsilon - 4y_1^2 - 4y_2^2) M^\sigma , \\
\frac{dM^\tau}{dl} &= (\epsilon - 4y_1^2 - 4y_3^2) M^\tau , \\
\frac{dM^m}{dl} &= (\epsilon - 4y_2^2 - 4y_3^2) M^m .
\end{aligned} \tag{S62}$$

where $M^m = \Gamma(\epsilon) g_m^2$.

Since our purpose is only to study the stability of the phase diagram Fig. 3(a) under small g_m , we only need to check the beta function:

$$\frac{dM^m}{dl} = (\epsilon - 4y_2^2 - 4y_3^2) M^m \tag{S63}$$

by which one can see only the spin and orbital KD fixed point **G** is unstable against a small M^m (and thus g_m), while the KS fixed point **K3**, spin or orbital KS fixed points **K2** and **K1**, the generic critical points **F1**, **F2**, and the multi-critical point **R1**, are stable against a weak coupling constant g_m .

As a result, the structure of the the phase diagram Fig. 3(a) remains unchanged, except now the spin and orbital KD phase correspond to the fixed point:

$$\mathbf{G}' : y_1 = y_2 = y_3 = 0, M^\sigma \rightarrow \infty, M^\tau \rightarrow \infty, M^m \rightarrow \infty$$

instead of **G**.